Introducing Cell Cycle Regulation to a Mathematical Model of the T-cell Proliferative Phase

Introducing Cell Cycle Regulation to a Mathematical Model of the T-cell Proliferative Phase

By Taran Bhartt, B.H.Sc. (Honours), M.A.Sc. candidate

A Thesis Submitted to the School of Graduate Studies in Partial Fulfilment of the Requirements for the Degree Master of Applied Science

McMaster University

M.A.Sc. Candidate McMaster University

Chemical Engineering Hamilton, Ontario, Canada

TITLE: Introducing Cell Cycle Regulation to a Mathematical Model of the T-cell Proliferative Phase

AUTHOR: Taran Bhartt B.H.Sc. and M.A.Sc. candidate

SUPERVISOR: Dr. Thomas A. Adams II

COSUPERVISOR: Dr. Prashant Mhaskar

NUMBER OF PAGES: xvi, 90

Lay Abstract

T-cells are an important component of the human immune system, but currently, there are no vaccines in clinical use that are designed to target them. This is because there are many different dynamics that underpin how T-cells activate, and to what degree they can replicate into a substantial pool of pathogen-clearing cells. Learning which candidate vaccines can properly elicit a strong T-cell response is time and resource consuming. Mathematical models can therefore speed development of candidate vaccines by virtually testing their T-cell responsiveness. This thesis works to improve on an existing mathematical model by introducing immunological mechanisms that determine how T-cells undergo cell division, change the acidity of their immediate surroundings, and respond to their own growing population. By doing so, this new model can be more representative of the immunological reality and begin to probe new dynamics of the T-cell response.

Abstract

CD8+ T cells are critical to the adaptive immune response and are a target for vaccine development. However, the complex dynamics of cell proliferation can vary response success, providing uncertainty when designing vaccines. Computer models can provide clarity by simulating these dynamics, tracking millions of cell-cell interactions, a feat that is impractical experimentally. Our group created the STORE.1 model, a probabilistic simulation of the CD8+ T cell response to vaccination. While able to accurately simulate in vivo mouse T cell clonal expansion, intracellular dynamics are absent. Furthermore, there is no mechanism by which cell division ceases. This work builds upon the STORE.1 model by systematically explaining the division dynamics of CD8+ T cells and providing measures of the extracellular environment. The new STORE.2 model has demonstrated an ability to accurately simulate differences in CD8+ T cell expansion in WT mice and mice lacking type I conventional dendritic cells up to 170 hours after vaccination. It is the first model to simulate individual cell cycle regulator protein counts for millions of cells, and the resulting impact on pH for the extracellular microenvironment. Finally, it provides a partial mechanism behind division cessation, an important element for future models seeking to further simulate the end of the T-cell response.

Acknowledgements

I would like to thank many, many people. As a newcomer to the field of computational biology, the guidance of my supervisors and peers was invaluable. I would like to thank my supervisor, Dr. Thomas A. Adams II, who took a chance on a health science student with absolutely no experience in chemical engineering. I would like to thank my committee members, Dr. Boyang Zhang, and Dr. Prashant Mhaskar, who took time out of their winter holiday break to read my thesis. I would like to thank the MACC and Adams group, particularly Nagat Elrefaei and Seyedeh Fatemeh "Nilou" Seyyedizadeh, who were not only fantastic collaborators, but friends whose humour and experience was invaluable; I have no doubt that their work on the STORE model will be truly significant. I would like to thank immunologists Dr. Ross M. Kedl and Dr. Christopher A. Hunter of the University of Colorado and University of Pennsylvania for all their hard laboratory work that underpins this project, but especially Dr. David Christian, who lent his invaluable perspective at countless biweekly meetings. I would like to thank the Canadian Institutes of Health Research, the Natural Sciences and Engineering Research Council, and the Social Sciences and Humanities Research Council for supporting this project financially. I would like to thank my friends and family. They lent me so much support every step of the process, whether it was talking shop about our respective research or taking necessary breaks for bad movie nights and board game cafes. Thank you to my parents, my little sister, Preeya, and my boyfriend, Myles, who have always shown more love, humour, and surgical deliveries of the word “plonker” than anyone could ask for. Thank you for being here every step of the way, from celebrating my acceptance to postponing a Mexico trip just to attend my defence. Finally, I would like to show my immense appreciation for the mice who gave their lives for the sake of our research. I hope it can help us reach a world where our clinical research can be less of a burden on both animal and human subjects.

Table of Contents

List of Figures

List of Tables

List of Abbreviations

Table 1: List of cell abbreviations used throughout the paper

Abbreviation	Definition
A	Naive OT-I T cell
AP	APC binding pairs with $Nur77^{GFP-}$ OT-I T cells
APC	Antigen Presenting Cell
B	T cell that has been primed after binding with a *P*
BP	APC binding pairs with $Nur77^{GFP+}$ OT-I T cells
C	Activated OT-I T cell that has separated from P and divided once
D	C-cell that has divided
E	D-cell that has divided
F	E-cell that has divided
G	F-cell that has divided
H	G-cell that has divided
I	H-cell that has divided
J	I-cell that has divided
K	E-J cell that have left the system

Abbreviation	Definition
A	Naive OT-I T cell
KO	An OT-I T-cell that was taken from a Wildtype mouse and inserted into a Knockout mouse
P	Antigen Presenting Cell
TCR	T-Cell Receptor
WT	An OT-I T-cell that was taken from a Wildtype mouse and inserted into a Wildtype mouse

Declaration of Academic Achievement

I, Taran Bhartt, state that the research presented in this document is my own work. It was performed under the supervision of Dr. Thomas A. Adams II. I am the sole author and researcher of this thesis. All data used for the construction of this model derives from previously published sources, and all facts are cited. All speculation is noted as such.

Chapter 1: Introduction

1.1 Background

1.1.1. The STORE Model

$CD8^+$ T cells are a critical element of the immune response, with the degree of T cell clonal expansion correlating with the elimination of pathogens such as HIV-AIDS, COVID-19, and malaria.[1-3] Thus, considerable, ongoing effort has been spent to develop vaccines that can elicit robust $CD8^+$ T cell proliferation.[3,4] However, both the availability of animal and human subjects for vaccine candidates, as well as the complex dynamics of cell proliferation have provided delays and uncertainty when designing vaccines.[5] Computer models can provide clarity by rapidly simulating these dynamics, tracking millions of cell-cell interactions for the next generation of vaccine candidates in ways that are difficult experimentally.[5]

Towards this aim, Christian et al. developed the STochastic Omentum REsponse (STORE) model, an agent-based black-box model that uses probabilities derived from literature and in vivo observations to accurately predict vaccine-induced $CD8^+$ T cell clonal expansion within the omentum up to 200 hours post vaccination.[6] The model uses six parameters: 1) the number of intraperitoneally transferred transgenic OVA-specific naive $CD8^+$ T cells (OT-I), 2) the ratio of transferred OT-I to the number of antigen presenting cells (APCs) activated by an OVA-expressing vaccine strain of the *T. gondii* parasite (*rAP*), the probabilities of 3) an OT-I and APC binding (*pAP,bind*), 4) an APC leaving the omentum (*pBP,leave*), 5) cells in divisions 3–6 leaving (*pEH,leave*), and 6) cells in divisions 7–8+ leaving the omentum (*pIJ,leave*).[6] Mitosis for divisions

1-6 utilize a probabilistic parameter based around a 5.3-hour division cycle, whereas subsequent divisions utilize a separate parameter based around a separate 24-hour division cycle.

1.1.2. The Cell Cycle

The cell cycle is the set of steps that allow a cell to reproduce clonally. The cell cycle is regulated by cyclins and cyclin-dependent kinases (CDKs). Cyclins are regulatory subunits of kinases, proteins capable of phosphorylation (the transfer of a high energy phosphate group to a protein). By tracking these regulators, it is possible to time out the length of the cell cycle.[7]

The first phase is G0, or quiescence. G0 is a state of arrest/inactivity that is distinct from interphase, the busy period where the cell performs its specialized tasks between divisions. Naive T-cells remain in G0 until activation. The time and metabolic requirements to leave G0 is one reason the first T-cell division takes much longer than subsequent divisions.[7]

G1, or the first gap phase, is part of a three-step process in preparation for mitosis, whereby cellular machinery duplicates.[7] There is a crucial checkpoint called the G1/S checkpoint, whereby cell machinery, namely the protein pair Cyclin E/CDK2, are upregulated if there has been enough production of metabolites to allow the cell to proceed to S phase.[7]

S phase is the DNA synthesis phase where the entire genome is duplicated. This phase can be detected by fluorescent 5-Ethynyl-2′-deoxyuridine (EdU) staining. EdU is incorporated into newly synthesizing DNA, allowing cells that have newly divided to be detected via flow cytometry.[7]

G2 is the final phase before cell division. There is one final checkpoint where Cyclin B/CDk1 ensures that the cell has produced enough metabolites, and grown large enough, to allow for cell division, or mitosis.[7]

1.1.3. c-MYC

A crucial attribute of the cell cycle is a rapid mobilization of metabolites. Cells must grow large enough to duplicate their entire nuclear DNA, divide without rupturing the cell envelope, and organize such that duplicated organelles are allocated between daughter cells to ensure that both remain viable.[8,9] This cellular process is an incredibly regulated series of changes, and requires substantial energy and resources to be marshalled.[9] One of the key players in the transcriptional regulation of this process is cellular-myelocytomatosis viral oncogene homologue (c-MYC).[10]

The c-MYC protein is a basic helix loop helix (bHLH) transcription factor that upregulates many metabolic pathways involving cell growth. By some estimates, the MYC family regulates 15% of all genes in the human genome.[11] c-MYC dysregulation can lead to the production of runaway growth/cancerous tumours, which is the context of much of its study. c-MYC is the prototypical member of the Myc family of transcription factors alongside N-MYC and L-MYC. While N-MYC and L-MYC show restricted expression during cell/tissue development, c-MYC is highly abundant in all manner of proliferating cells and is of particular importance for immune cell proliferation.[12,13]

c-MYC serves as a rate-limiting factor for the G1/S transition of the cell cycle, and without c-MYC, cells enter G0, with impaired c-MYC functioning results in a prolonged G1 and G2 phase with an unaffected S phase.[14,15] There is evidence that other growth factors such as cellular Src is capable of rescuing early steps of the G1/S phase transition, but it ultimately fails to activate the late stage regulators, such as cyclins E and Cdk2, or cyclins A and Cdk2: the different regulators having varying relevance depending upon the cellular context, and yet c-MYC remains integral.[14] Ultimately, given its role in upregulating numerous biosynthetic pathways, the cell would not have produced the necessary cellular contents of the G1 replicative phase to progress into the DNA

synthetic S-phase.[16] Additional c-MYC can rescue a cell arrested in G0, prompting it to progress through G1. Naive T-cells sit in G0 until activated, and there is evidence that CD8+ T-cells emerge from G0 more readily than CD4+ T-cells, progressing through the cell cycle at roughly twice the speed when strongly stimulated by PMA, ionomycin, and anti-CD28 monoclonal antibodies.[17]

Quiescent/G0 naive T-cells have low metabolic demands, utilizing the efficient but slow oxidative phosphorylation and fatty acid metabolism to sustain mere survival in their minimally active state.[19] It is only with activation that their increased energetic needs provoke the additional use of the less efficient but quicker glutaminolysis and glycolysis pathways.[16,18] This transition to "speedier" metabolic pathways is mirrored by extremely proliferative tumour cells, which are also rich in c-MYC.[19]

Naive T-cells clonally expand before developing effector subtypes, with the glycolytic metabolism likely tied to c-MYC expression.[20] Furthermore, upregulated c-MYC driven glutaminolysis produces polyamines that are essential to T-cell proliferation, with c-MYC deleted cells not growing to the same size as their fully functional counterparts.[21]

c-MYC can elevate glycolysis by up to 20% during the induction of cell division (G0 to G1), with the elevated energy production essential to transitioning T-cells into S phase.[22]

There is a wide range of metabolic profiles employed by memory T-cells. Effector memory T-cells still utilize glycolysis to a large degree, while resident and central memory T-cells rely less on glycolysis and glutaminolysis pathways, transitioning towards fatty acid metabolism.[18,23] c-MYC gene knockout mouse fibroblast cells were found to upregulate fatty acid metabolism to compensate for the loss of glycolytic metabolism.[24]

As part of c-MYC's upregulation of protein synthesis, there is an increase in mitochondrial mass, along with an increase in mitochondrial function. During entry into the cell cycle, c-MYC

positive cells can show a three-to-four-fold increase in oxygen consumption compared to c-MYC deleted cells, as well as higher mitochondrial membrane potential (a sign of increased hydrogen pumping to fuel oxidative phosphorylation).[25]

c-MYC functions to promote the cell cycle through a number of ways. In addition to upregulating metabolic genes to provide the cell with the energy and nutrients necessary to progress through each stage of the cell cycle, it also regulates a host of proteins that progress the cell cycle through activator or repressor activity, as well as antagonizing cell cycle brakes, proteins that act to arrest the cell cycle.[26] c-MYC can operate on the transcriptional level, preventing cell cycle brakes such as p15, p21, and p27 from being transcribed and translated from DNA to proteins, as well as upregulating inhibitors to enhance the degradation of p27 via ubiquitin ligases complexes.[26]

When it comes to S-phase, the phase of the cell cycle where DNA is replicated, the duration appears to be determined by c-MYC.[27] Control human fibroblasts completed S-phase in 5-6 hours, whereas fibroblasts with elevated c-MYC completed S-phase in 3-4 hours, indicating that c-Myc overexpression accelerates the progression of S-phase by approximately 40% in normal human fibroblasts.[28] A rat fibroblast cell line completed S-phase in 11 hours, whereas rat fibroblasts with knocked out c-MYC took 14 hours. When rat fibroblasts lacking c-MYC were given retroviral c-MYC, S-phase was completed in 6 hours.[28] Thus, c-MYC not only rescued S-phase from delay, but accelerated it nearly two fold relative to the wild type cells.[28] Similarly, c-MYC deletion in rat fibroblasts lengthens G1 and G2 while leaving the duration of S-phase unaffected.[29] Thus, it is important to map c-MYC dynamics over the course of the cell cycle, and the entire proliferative phase in order to predict the degree of $CD8^+$ T cell clonal expansion.

1.1.4. c-MYC Determinants

c-MYC concentration in $CD8^+$ T cells can be considered division independent, as c-MYC levels remain stable across generations at any particular time point.[30] c-MYC levels decline primarily due to negative feedback loops and degradation mechanisms, rather than being halved during mitosis.[30] c-MYC levels are sustained by similarly rapid production and degradation rates that are independent of cell age and generation.[30] These production rates are inherited by daughter cells that quickly re-establish c-MYC turnover equilibrium following division.[30] In this way, c-MYC level decline is due to changes in production rates that do not correlate with which generation a cell belongs to.[30]

The role of c-MYC in $CD8^+$ T cell proliferation begins following naive T cell activation. c-MYC is upregulated immediately following T cell receptor (TCR) stimulation by APCs presenting cognate antigen. TCR activation elicits a fixed pool of c-MYC depending on the antigen affinity, and c-MYC production is further heightened by APC costimulation and cytokines in the extracellular microenvironment.[30,31]

Antigen affinity for the TCR is a quotient of the rate constants for antigen binding and dissociation (k_{on} and k_{off}).[32] Antigen affinity for the TCR is a continuum, but activation is a binary process, with a threshold that antigens must clear if a cell is to initiate proliferation, though it is a threshold that is not static but can be raised or lowered by cytokines, costimulation, and the physical/chemical properties of the antigen.[33,34]

Following immunization with CPS parasites, the initial APCs were infected macrophages in the omentum while antigen presentation by cDC1 was also required for a robust OT-I T cell response. [6] cDC1s and macrophages are a critical source of IL-12 during T. gondii infection.[35-37] They are also a crucial source of IL-27 after subunit immunization with a combined adjuvant.[38-40]

IL-27 production by cDC1 and monocytes hours after immunization has been shown to predict the magnitude of CD8+ T cell proliferation seven days after immunization, as well as the degree of activity and immune memory.[38,41-42,] IL-27 interacts with T cells via the STAT1 and STAT3 transcription factors, the latter of which binds to the promoter of the c-Myc gene.[43,44] Overall cDC1 cytokine production occurs as a transitory pulse several hours after stimulation by TLR ligands and CD40L, and is subsequently coupled with increasing expression of the costimulatory molecules CD80 and CD86 that is capable of providing a more potent stimulation of T cells that results in increased c-Myc expression.[31,45-47]

Whether the impetus is TCR-stimulation or cytokine production, the downstream mechanism is identical: upregulation of c-MYC mRNA transcription. In this way, activation of the TCR produces some baseline increase in c-MYC, with additional c-MYC being the product of cytokine expression.

As part of upregulating metabolic pathways, c-MYC engages with positive feedback loops. c-MYC activity is so tied to amino acid transporter activity that the deletion of individual c-MYC-controlled amino acid transporters will functionally phenocopy the effects of c-Myc deletion.[48] c-MYC induces reprogramming of the T-cell proteome by upregulating amino acid transporters, producing knock-on effects for biosynthetic and bioenergetic pathways.[48]

Following naïve T cell activation, c-Myc selectively shapes T cell phenotypes by licensing T cell receptor driven proteome reprogramming including the upregulation of cell surface amino acid transporters. c-MYC thus engages in a positive feedback loop increasing extracellular amino acid (EAA) transport into the cell, which in turn is necessary for further c-MYC production.[31] Specifically, c-MYC activates transcription of key transporters such as solute carrier family (SLC) 7 member 5 (SLC7A5) and SLC43A1 that import EAAs that stimulate c-Myc mRNA

translation.[49,50] Furthermore, c-MYC upregulates lactate transporter expression that enables metabolic flux towards glutaminolysis and glycolysis.[50] Glycolysis and glutaminolysis increases transport of excess glucose and glutamine towards the hexamine biosynthetic pathway which produces (UDP)-GlcNAc that acts as a stabilizing agent for proteins such as c-MYC.[50] This positive feedback loop sustains cell proliferative metabolism, and opposes c-MYC degradation.[48]

Furthermore, c-MYC upregulates lactate transporter expression that enables metabolic flux towards glutaminolysis and glycolysis. Glycolysis and glutaminolysis increases transport of excess glucose and glutamine towards the hexamine biosynthetic pathway which produces (UDP)-GlcNAc. (UDP)-GlcNAc acts as a stabilizing agent for proteins such as c-MYC.[50]

The levels of c-Myc expression in T cells are controlled in part by impairing the positive feedback loop via the production of lactic acid byproducts of glycolysis that cause an acidic niche within lymphoid tissue.[52] The resulting lower pH temporarily impairs monocarboxylate transporter function and reduces glycolytic flux that decreases (UDP)-GlcNAc stabilization of c-MYC.[51,52] Acidic microenvironments also downregulate SLC7A5 expression in $CD8^+$ T cells, removing a key source of EAA and thus decreasing c-Myc production.[53] The pH of the lymphoid tissue is stabilized as lower c-Myc levels decrease glycolysis and shunts the production of lactic acid, and lactic acid is cleared via the bicarbonate buffering.[52] Crucially, while acidification impairs activated $CD8^+$ T cell metabolism, acidification does not impair further dendritic cell activation of naive T cells.[52]

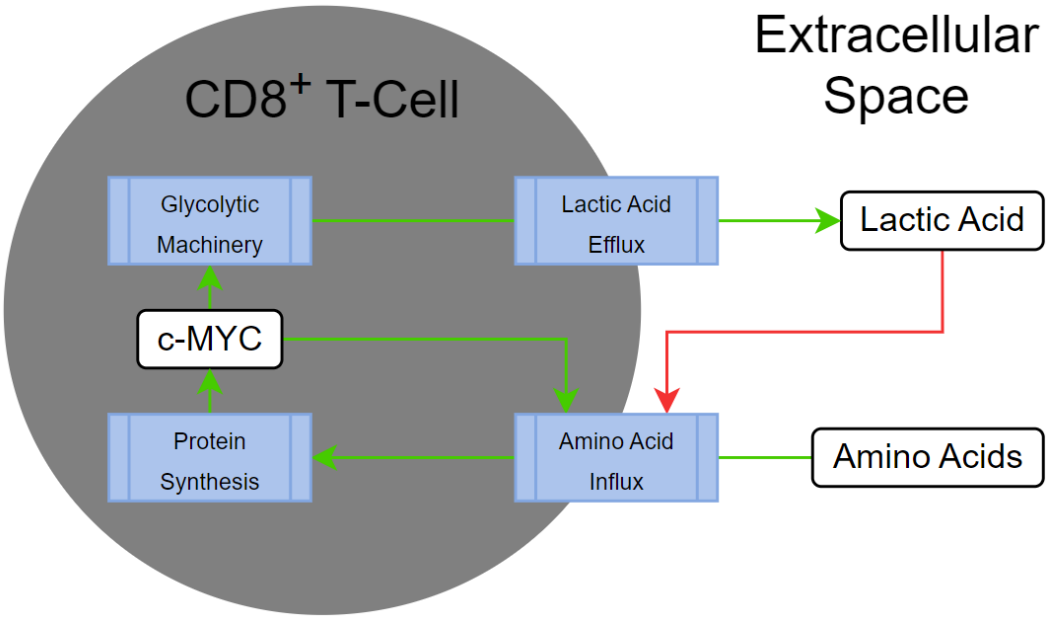

Figure 1: Diagram of how c-MYC generates positive (green) and negative (red) feedback loops that augments the number of c-MYC proteins.

While acidification impairs c-MYC positive feedback, c-MYC levels also decrease by several different mechanisms of protein degradation. c-MYC can be broken down via the ubiquitin-proteasome pathway, whereby c-MYC marked with ubiquitin polypeptides is rapidly degraded by the 26S proteasome.[54] When ubiquitination target sites on the c-MYC protein are modified, the half-life increases from 35 minutes to 2.5 hours.[54]

The ubiquitin-proteasome pathway is composed of 3 enzymes that work in concert to attach ubiquitin polypeptides to lysine residues on the target protein, in this case, c-MYC. Once marked by multiubiquitination, c-MYC proteins are quickly degraded by the 26S proteasome.[54]

There is also another mechanism for degradation. A region of the c-MYC protein called the PEST region, is a key target for degradation.[54]

Finally, the N-terminal region of the protein is a target of ubiquitination, which marks the protein for degradation by proteasomes. When the N-terminal was modified, the in vivo c-MYC half-life increased from 35 minutes to 2.5 hours.[54]

The timing of ubiquitination within the cell cycle is further explored by Sears et al. They explore how c-MYC protein is further regulated at two amino acids: Serine 62, and Threonine 58.[55] c-MYC is stabilized by phosphorylated Serine 62 and destabilized by phosphorylated Threonine 58. Following TCR activation, a chain of proteins called the MAPK/ERK pathway is activated, upregulating several pro-proliferation proteins, one of which is c-MYC. MAPK/ERK phosphorylates Serine 62, and prevents the phosphorylation of Threonine 58 via signalling of the Akt-pathway (another pro-proliferation pathway that is upregulated following TCR activation), allowing increased c-MYC stability into G1. Later in the G1 phase, Akt signalling wanes, allowing for Threonine-58 to become phosphorylated, and destabilize c-MYC.[55-57]

Gooken et al. find that c-MYC protein is greater during G1 than G0, and that indeed, c-MYC levels rise and then fall over the course of G1, but they also determine that c-MYC levels continue to rise over the course of S-phase and G2 to reach a peak value at G2/M, before declining back to the new G1 baseline.[58]

Whereas other data suggests that c-MYC is most elevated during S-phase. Quantifications of c-MYC levels in B-cells over different cell cycle phases suggest c-MYC expression is elevated in all phases relative to inactive cells, but reaches peak expression during S-phase (20- to 40-fold increase during S phase compared to only a 5- to 20-fold increase during other phases from the baseline of inactive cells).[59]

The overall pattern is of WT c-MYC being substantially low in quiescent cells, rising in activated pre-mitotic cells, then declining during mitosis with a half-life of approximately 35

minutes before increasing once more during G1-G2. While c-MYC is division independent, it is cell-cycle dependent.

Once c-MYC levels have dropped, its activity is maintained by the transcription factor AP4. AP4 is dependent upon TCR signalling via downstream c-MYC directly binding to AP4, and sustained IL-2 signalling for gene transcription and post translational modifications.[60] Temporally, AP4 is upregulated at roughly the same time as c-MYC, but only begins to decline once c-MYC has already significantly degraded (90%).[60] Furthermore, the gene profiles for AP4 and c-MYC overlap substantially (~75%), resulting in a handoff from c-MYC to AP4, and thus ensuring that CD8+ T cells continue to benefit from the proliferative and energetic pathways that were originally initiated by c-MYC. [60] AP4 finally declines in step with the slowing T cell expansion. [60]

1.2. Thesis Contribution - The STORE.2 Model

Intracellular dynamics are absent in the STORE.1 model, with cell division deriving from population-level observations. Furthermore, there is no mechanism through which division can cease. This work builds upon the STORE model by systematically explaining the transition time for CD8+ T cells. This new model replaces the division probabilities by simulating intracellular cell cycle regulators as a function of changes within the cellular microenvironment and cytokine expression by APCs. A breakdown of the STORE.2 model parameters and functions are detailed in 2.1. and 2.2.

The STORE.2 model simulates, for the first time, the absolute number of c-MYC proteins in every individual cell. Consequently, it introduces to the STORE group of models a measure of metabolism, the length of pre-mitosis, and the acidity of the local microenvironment. Importantly, despite using a new mechanism for cell division, the STORE.2 model can accurately simulate OT-I

CD8+ clonal expansion for WT and KO mice like the previous STORE.1 model, demonstrating that the increased explanatory power does not come at the expense of predictive power.

1.3. References

1) McMichael, Andrew J, and Wayne C Koff. “Vaccines That Stimulate T Cell Immunity to HIV-1: The next Step.” *Nature Immunology* 15, no. 4 (March 19, 2014): 319–22. https://doi.org/10.1038/ni.2844.
2) Gilbert, Sarah C. “T-Cell-Inducing Vaccines - What’s the Future.” *Immunology* 135, no. 1 (December 7, 2011): 19–26. https://doi.org/10.1111/j.1365-2567.2011.03517.x.
3) Huang, Huang, Michael J. Sikora, Saiful Islam, Roshni Roy Chowdhury, Yueh-hsiu Chien, Thomas J. Scriba, Mark M. Davis, and Lars M. Steinmetz. “Select Sequencing of Clonally Expanded CD8+ T Cells Reveals Limits to Clonal Expansion.” *Proceedings of the National Academy of Sciences* 116, no. 18 (April 30, 2019): 8995–9001. https://doi.org/10.1073/pnas.1902649116.
4) Ura, Takehiro, Masaki Takeuchi, Tatsukata Kawagoe, Nobuhisa Mizuki, Kenji Okuda, and Masaru Shimada. “Current Vaccine Platforms in Enhancing T-Cell Response.” *Vaccines* 10, no. 8 (August 1, 2022): 1367. https://doi.org/10.3390/vaccines10081367.
5) Handel, Andreas, Nicole L La, and Paul G Thomas. “Simulation Modelling for Immunologists.” *Nature Reviews Immunology* 20, no. 3 (December 5, 2019): 186–95. https://doi.org/10.1038/s41577-019-0235-3.
6) Christian, David A, Thomas A Adams, Lindsey Shallberg, Anthony T Phan, Tony E Smith, Mosana Abraha, Joseph W Perry, et al. “CDC1 Coordinate Innate and Adaptive Responses in the Omentum Required for T Cell Priming and Memory.” *Science Immunology* 7, no. 75 (September 30, 2022). https://doi.org/10.1126/sciimmunol.abq7432.
7) Matthews, Helen K., Cosetta Bertoli, and Robertus A. M. de Bruin. “Cell Cycle Control in Cancer.” *Nature Reviews Molecular Cell Biology* 23 (September 10, 2021). https://doi.org/10.1038/s41580-021-00404-3.
8) Chang, J. T., V. R. Palanivel, I. Kinjyo, F. Schambach, A. M. Intlekofer, A. Banerjee, S. A. Longworth, et al. “Asymmetric T Lymphocyte Division in the Initiation of Adaptive Immune

Responses." *Science* 315, no. 5819 (March 23, 2007): 1687–91. https://doi.org/10.1126/science.1139393.

9) Kalucka, Joanna, Rindert Missiaen, Maria Georgiadou, Sandra Schoors, Christian Lange, Katrien De Bock, Mieke Dewerchin, and Peter Carmeliet. "Metabolic Control of the Cell Cycle." *Cell Cycle* 14, no. 21 (October 2, 2015): 3379–88. https://doi.org/10.1080/15384101.2015.1090068.
10) MYC MYC proto-oncogene, bHLH transcription factor [Homo sapiens (human)] [Internet]. Bethesda (MD): National Library of Medicine (US), National Center for Biotechnology Information; 2004 – [cited 2023 12 03]. Available from: https://www.ncbi.nlm.nih.gov/gene/4609
11) Dang, Chi V., Kathryn A. O'Donnell, Karen I. Zeller, Tam Nguyen, Rebecca C. Osthus, and Feng Li. "The C-Myc Target Gene Network." *Seminars in Cancer Biology* 16, no. 4 (August 1, 2006): 253–64. https://doi.org/10.1016/j.semcancer.2006.07.014.
12) Madden, Sarah K., Aline Dantas de Araujo, Mara Gerhardt, David P. Fairlie, and Jody M. Mason. "Taking the Myc out of Cancer: Toward Therapeutic Strategies to Directly Inhibit C-Myc." *Molecular Cancer* 20, no. 1 (January 4, 2021). https://doi.org/10.1186/s12943-020-01291-6.
13) Gnanaprakasam, J.N. Rashida, and Ruoning Wang. "MYC in Regulating Immunity: Metabolism and Beyond." *Genes* 8, no. 3 (February 24, 2017): 88. https://doi.org/10.3390/genes8030088.
14) Prathapam, Tulsiram, Sarah Tegen, Thordur Oskarsson, Andreas Trumpp, and G. Steven Martin. "Activated Src Abrogates the Myc Requirement for the G_0 /G_1 Transition but Not for the G_1 /S Transition." *Proceedings of the National Academy of Sciences* 103, no. 8 (February 13, 2006): 2695–2700. https://doi.org/10.1073/pnas.0511186103.
15) Dang, Chi V. "C-Myc Target Genes Involved in Cell Growth, Apoptosis, and Metabolism." *Molecular and Cellular Biology* 19, no. 1 (January 1, 1999): 1–11. https://www.ncbi.nlm.nih.gov/pmc/articles/PMC83860/.
16) Veiga Moreira, Jorgelindo da, Sabine Peres, Jean-Marc Steyaert, Erwan Bigan, Loïc Paulevé, Marcel Levy Nogueira, and Laurent Schwartz. "Cell Cycle Progression Is Regulated by Intertwined Redox Oscillators." *Theoretical Biology and Medical Modelling* 12, no. 1 (May 29, 2015). https://doi.org/10.1186/s12976-015-0005-2.

17) Mishima, Takuya, Shotaro Fukaya, Shoko Toda, Yoshiaki Ando, Tsukasa Matsunaga, and Manabu Inobe. “Rapid G0/1 Transition and Cell Cycle Progression in CD8+ T Cells Compared to CD4+ T Cells Following in Vitro Stimulation.” *Microbiology and Immunology* 61, no. 5 (May 2017): 168–75. https://doi.org/10.1111/1348-0421.12479.

18) Zhang, Lianjun, and Pedro Romero. “Metabolic Control of CD8+ T Cell Fate Decisions and Antitumor Immunity.” *Trends in Molecular Medicine* 24, no. 1 (January 1, 2018): 30–48. https://doi.org/10.1016/j.molmed.2017.11.005.

19) Goetzman, Eric S., and Edward V. Prochownik. “The Role for Myc in Coordinating Glycolysis, Oxidative Phosphorylation, Glutaminolysis, and Fatty Acid Metabolism in Normal and Neoplastic Tissues.” *Frontiers in Endocrinology* 9 (April 12, 2018). https://doi.org/10.3389/fendo.2018.00129.

20) Brenchley, J. M., D. C. Douek, D. R. Ambrozak, M. Chatterji, M. R. Betts, L. S. Davis, And R. A. Koup. “Expansion of Activated Human Naïve T-Cells Precedes Effector Function.” *Clinical & Experimental Immunology* 130, no. 3 (November 24, 2002): 432–40. https://doi.org/10.1046/j.1365-2249.2002.02015.x.

21) Windt, Gerritje J. W., and Erika L. Pearce. “Metabolic Switching and Fuel Choice during T-Cell Differentiation and Memory Development.” *Immunological Reviews* 249, no. 1 (August 14, 2012): 27–42. https://doi.org/10.1111/j.1600-065x.2012.01150.x.

22) Greiner, E F, M Guppy, and K Brand. “Glucose Is Essential for Proliferation and the Glycolytic Enzyme Induction That Provokes a Transition to Glycolytic Energy Production.” *Journal of Biological Chemistry* 269, no. 50 (December 1994): 31484–90. https://doi.org/10.1016/s0021-9258(18)31720-4.

23) O’Sullivan, David. “The Metabolic Spectrum of Memory T Cells.” *Immunology & Cell Biology* 97, no. 7 (June 12, 2019): 636–46. https://doi.org/10.1111/imcb.12274.

24) Edmunds, Lia R, Lokendra Kumar Sharma, Audry Kang, Jie Lu, Jerry Vockley, Shrabani Basu, Radha Uppala, et al. “C-Myc Programs Fatty Acid Metabolism and Dictates Acetyl-CoA Abundance and Fate.” *Journal of Biological Chemistry* 289, no. 36 (September 1, 2014): 25382–92. https://doi.org/10.1074/jbc.m114.580662.

25) Morrish, F., and D. Hockenbery. “MYC and Mitochondrial Biogenesis.” *Cold Spring Harbor Perspectives in Medicine* 4, no. 5 (May 1, 2014): a014225–25. https://doi.org/10.1101/cshperspect.a014225.

26) García-Gutiérrez, Lucía, María Dolores Delgado, and Javier León. “MYC Oncogene Contributions to Release of Cell Cycle Brakes.” *Genes* 10, no. 3 (March 22, 2019): 244. https://doi.org/10.3390/genes10030244.

27) Takeda, David Y, and Anindya Dutta. “DNA Replication and Progression through S Phase.” *Oncogene* 24, no. 17 (April 2005): 2827–43. https://doi.org/10.1038/sj.onc.1208616.

28) Robinson, Kristin, Nichaya Asawachaicharn, Denise A. Galloway, and Carla Grandori. “C-Myc Accelerates S-Phase and Requires WRN to Avoid Replication Stress.” Edited by Mikhail V. Blagosklonny. *PLoS ONE* 4, no. 6 (June 18, 2009): e5951. https://doi.org/10.1371/journal.pone.0005951.

29) Mateyak, M. K., A. J. Obaya, S. Adachi, and J. M. Sedivy. “Phenotypes of C-Myc-Deficient Rat Fibroblasts Isolated by Targeted Homologous Recombination.” *Cell Growth & Differentiation: The Molecular Biology Journal of the American Association for Cancer Research* 8, no. 10 (October 1, 1997): 1039–48. https://pubmed.ncbi.nlm.nih.gov/9342182/.

30) Heinzel, Susanne, Tran Binh Giang, Andrey Kan, Julia M. Marchingo, Bryan K. Lye, Lynn M. Corcoran, and Philip D. Hodgkin. “A Myc-Dependent Division Timer Complements a Cell-Death Timer to Regulate T Cell and B Cell Responses.” *Nature Immunology* 18, no. 1 (January 1, 2017): 96–103. https://doi.org/10.1038/ni.3598.

31) Preston, Gavin C, Linda V Sinclair, Aneesa Kaskar, Jens L Hukelmann, Maria N Navarro, Isabel Ferrero, H Robson MacDonald, Victoria H Cowling, and Doreen A Cantrell. “Single Cell Tuning of Myc Expression by Antigen Receptor Signal Strength and Interleukin-2 in T Lymphocytes.” *The EMBO Journal* 34, no. 15 (July 2015): 2008–24. https://doi.org/10.15252/embj.201490252.

32) Stone, Jennifer D., Adam S. Chervin, and David M. Kranz. “T-Cell Receptor Binding Affinities and Kinetics: Impact on T-Cell Activity and Specificity.” *Immunology* 126, no. 2 (February 2009): 165–76. https://doi.org/10.1111/j.1365-2567.2008.03015.x.

33) Elliot, Thomas A. E., Emma K. Jennings, David A. J. Lecky, Natasha Thawait, Adriana Flores-Langarica, Alastair Copland, Kendle M. Maslowski, David C. Wraith, and David Bending. “Antigen and Checkpoint Receptor Engagement Recalibrates T Cell Receptor Signal Strength.” *Immunity* 54, no. 11 (November 9, 2021): 2481-2496.e6. https://doi.org/10.1016/j.immuni.2021.08.020.

34) Gallagher, M J, James Conley, and Leslie J Berg. “Peptide Antigen Concentration Modulates Digital NFAT1 Activation in Primary Mouse Naive CD8+ T Cells as Measured by Flow Cytometry of Isolated Cell Nuclei.” *ImmunoHorizons* 2, no. 7 (August 1, 2018): 208–15. https://doi.org/10.4049/immunohorizons.1800032.

35) Mashayekhi, Mona, Michelle M. Sandau, Ildiko R. Dunay, Eva M. Frickel, Asis Khan, Romina S. Goldszmid, Alan Sher, et al. “CD8α+ Dendritic Cells Are the Critical Source of Interleukin-12 That Controls Acute Infection by Toxoplasma Gondii Tachyzoites.” *Immunity* 35, no. 2 (August 2011): 249–59. https://doi.org/10.1016/j.immuni.2011.08.008.

36) Arango Duque, Guillermo, and Albert Descoteaux. “Macrophage Cytokines: Involvement in Immunity and Infectious Diseases.” *Frontiers in Immunology* 5, no. 491 (October 7, 2014). https://doi.org/10.3389/fimmu.2014.00491.

37) Hsieh, C., S. Macatonia, C. Tripp, S. Wolf, A O’Garra, and K. Murphy. “Development of TH1 CD4+ T Cells through IL-12 Produced by Listeria-Induced Macrophages.” *Science* 260, no. 5107 (April 23, 1993): 547–49. https://doi.org/10.1126/science.8097338.

38) Kilgore, Augustus M., Nathan D. Pennock, and Ross M. Kedl. “CDC1 IL-27p28 Production Predicts Vaccine-Elicited CD8+ T Cell Memory and Protective Immunity.” *The Journal of Immunology* 204, no. 3 (December 23, 2019): 510–17. https://doi.org/10.4049/jimmunol.1901357.

39) Abdalla, Abualgasim Elgaili, Qiming Li, Longxiang Xie, and Jianping Xie. “Biology of IL-27 and Its Role in the Host Immunity against Mycobacterium Tuberculosis.” *International Journal of Biological Sciences* 11, no. 2 (2015): 168–75. https://doi.org/10.7150/ijbs.10464.

40) Liu, Jianguo, Xiuqin Guan, and Xiaojing Ma. “Regulation of IL-27 P28 Gene Expression in Macrophages through MyD88- and Interferon-γ–Mediated Pathways.” *Journal of Experimental Medicine* 204, no. 1 (January 16, 2007): 141–52. https://doi.org/10.1084/jem.20061440.

41) Kilgore, Augustus M., Seth Welsh, Elizabeth E. Cheney, Alisha Chitrakar, Trevor J. Blain, Benjamin J. Kedl, Chris A. Hunter, Nathan D. Pennock, and Ross M. Kedl. “IL-27p28 Production by XCR1+ Dendritic Cells and Monocytes Effectively Predicts Adjuvant-Elicited CD8+ T Cell Responses.” *ImmunoHorizons* 2, no. 1 (January 1, 2018): 1–11. https://doi.org/10.4049/immunohorizons.1700054.

42) Pennock, Nathan D, Laurent Gapin, and Ross M Kedl. “IL-27 Is Required for Shaping the Magnitude, Affinity Distribution, and Memory of T Cells Responding to Subunit

Immunization." *Proceedings of the National Academy of Sciences of the United States of America* 111, no. 46 (September 29, 2014): 16472–77. https://doi.org/10.1073/pnas.1407393111.

43) Kiuchi, Nobuo, Koichi Nakajima, Makoto Ichiba, Toshiyuki Fukada, Masahiro Narimatsu, Katsunori Mizuno, Masahiko Hibi, and Toshio Hirano. "STAT3 Is Required for the Gp130-Mediated Full Activation of the C-Myc Gene." *Journal of Experimental Medicine* 189, no. 1 (January 4, 1999): 63–73. https://doi.org/10.1084/jem.189.1.63.

44) Owaki, Toshiyuki, Masayuki Asakawa, Noriko Morishima, Izuru Mizoguchi, Fumio Fukai, Kiyoshi Takeda, Junichiro Mizuguchi, and Takayuki Yoshimoto. "STAT3 Is Indispensable to IL-27-Mediated Cell Proliferation but Not to IL-27-Induced Th1 Differentiation and Suppression of Proinflammatory Cytokine Production." *The Journal of Immunology* 180, no. 5 (February 21, 2008): 2903–11. https://doi.org/10.4049/jimmunol.180.5.2903.

45) Hokey, David A., Adriana T. Larregina, Geza Erdos, Simon C. Watkins, and Louis D. Falo. "Tumor Cell Loaded Type-1 Polarized Dendritic Cells Induce Th1-Mediated Tumor Immunity." *Cancer Research* 65, no. 21 (November 1, 2005): 10059–67. https://doi.org/10.1158/0008-5472.can-05-1692.

46) Langenkamp, Anja, Mara Messi, Antonio Lanzavecchia, and Federica Sallusto. "Kinetics of Dendritic Cell Activation: Impact on Priming of TH1, TH2 and Nonpolarized T Cells." *Nature Immunology* 1, no. 4 (October 2000): 311–16. https://doi.org/10.1038/79758.

47) Marchingo, Julia M., Andrey Kan, Robyn M. Sutherland, Ken R. Duffy, Cameron J. Wellard, Gabrielle T. Belz, Andrew M. Lew, Mark R. Dowling, Susanne Heinzel, and Philip D. Hodgkin. "Antigen Affinity, Costimulation, and Cytokine Inputs Sum Linearly to Amplify T Cell Expansion." *Science* 346, no. 6213 (November 28, 2014): 1123–27. https://doi.org/10.1126/science.1260044.

48) Marchingo, Julia M, Linda V Sinclair, Andrew JM Howden, and Doreen A Cantrell. "Quantitative Analysis of How Myc Controls T Cell Proteomes and Metabolic Pathways during T Cell Activation." Edited by Ellen A Robey, Tadatsugu Taniguchi, Ellen A Robey, and Jeroen P Roose. *ELife* 9 (February 5, 2020): e53725. https://doi.org/10.7554/eLife.53725.

49) Ming, Yue, Jue Jiang, Peng Gao, Hudan Liu, and Guoliang Qing. "Oncogenic MYC Activates a Feedforward Regulatory Loop Promoting Essential Amino Acid Metabolism and

Tumorigenesis." *Cell Reports* 21, no. 13 (December 1, 2017): 3819–32. https://doi.org/10.1016/j.celrep.2017.12.002.

50) Yang, Luming, Zhaole Chu, Meng Liu, Qiang Zou, Juanjuan Li, Qin Liu, Yazhou Wang, Tao Wang, Junyu Xiang, and Bin Wang. "Amino Acid Metabolism in Immune Cells: Essential Regulators of the Effector Functions, and Promising Opportunities to Enhance Cancer Immunotherapy." *Journal of Hematology & Oncology* 16, no. 1 (June 5, 2023). https://doi.org/10.1186/s13045-023-01453-1.
51) Swamy, Mahima, Shalini Pathak, Katarzyna M. Grzes, Sebastian Damerow, Linda V. Sinclair, Daan M. F. van Aalten, and Doreen A. Cantrell. "Glucose and Glutamine Fuel Protein O-GlcNAcylation to Control T Cell Self-Renewal and Malignancy." *Nature Immunology* 17, no. 6 (June 1, 2016): 712–20. https://doi.org/10.1038/ni.3439.
52) Wu, Hao, Veronica Estrella, Matthew Beatty, Dominique Abrahams, Asmaa El-Kenawi, Shonagh Russell, Arig Ibrahim-Hashim, et al. "T-Cells Produce Acidic Niches in Lymph Nodes to Suppress Their Own Effector Functions." *Nature Communications* 11, no. 1 (August 17, 2020): 4113. https://doi.org/10.1038/s41467-020-17756-7.
53) Cheng, Hongcheng, Yajing Qiu, Yue Xu, Lan Chen, Kaili Ma, Mengyuan Tao, Luke Frankiw, et al. "Extracellular Acidosis Restricts One-Carbon Metabolism and Preserves T Cell Stemness." *Nature Metabolism* 5, no. 2 (January 30, 2023): 314–30. https://doi.org/10.1038/s42255-022-00730-6.
54) Gregory, Mark A., and Stephen R. Hann. "C-Myc Proteolysis by the Ubiquitin-Proteasome Pathway: Stabilization of C-Myc in Burkitt's Lymphoma Cells." *Molecular and Cellular Biology* 20, no. 7 (April 1, 2000): 2423–35. https://www.ncbi.nlm.nih.gov/pmc/articles/PMC85426/#:~:text=Degradation%20and%20ubiquitination%20of%20c%2DMyc%20are%20inhibited%20in%20mitotic%20cells.
55) Sears, Rosalie, Gustavo Leone, James DeGregori, and Joseph R Nevins. "Ras Enhances Myc Protein Stability." *Molecular Cell* 3, no. 2 (February 1999): 169–79. https://doi.org/10.1016/s1097-2765(00)80308-1.
56) Sears, Rosalie, Faison Nuckolls, Eric Haura, Yoichi Taya, Katsuyuki Tamai, and Joseph R. Nevins. "Multiple Ras-Dependent Phosphorylation Pathways Regulate Myc Protein Stability." *Genes & Development* 14, no. 19 (October 1, 2000): 2501–14. https://www.ncbi.nlm.nih.gov/pmc/articles/PMC316970/.

57) Sears, Rosalie C. “The Life Cycle of C-Myc: From Synthesis to Degradation.” *Cell Cycle* 3, no. 9 (September 9, 2004): 1131–35. https://doi.org/10.4161/cc.3.9.1145.

58) Gookin, Sara, Mingwei Min, Harsha Phadke, Mingyu Chung, Justin Moser, Iain Miller, Dylan Carter, and Sabrina L. Spencer. “A Map of Protein Dynamics during Cell-Cycle Progression and Cell-Cycle Exit.” Edited by Jonathon Pines. *PLOS Biology* 15, no. 9 (September 11, 2017): e2003268. https://doi.org/10.1371/journal.pbio.2003268.

59) Lacy, J, S N Sarkar, and W C Summers. “Induction of C-Myc Expression in Human B Lymphocytes by B-Cell Growth Factor and Anti-Immunoglobulin.” *Proceedings of the National Academy of Sciences* 83, no. 5 (March 1986): 1458–62. https://doi.org/10.1073/pnas.83.5.1458.

60) Chou, Chun, Amelia K. Pinto, Jonathan D. Curtis, Stephen P. Persaud, Marina Cella, Chih-Chung Lin, Brian T. Edelson, et al. “C-Myc-Induced Transcription Factor AP4 Is Required for Host Protection Mediated by CD8+ T Cells.” *Nature Immunology* 15, no. 9 (September 1, 2014): 884–93. https://doi.org/10.1038/ni.2943.

Chapter 2: STORE.2

2.1. Terminology

Table 2: List of User-Supplied Parameters

Parameter	Definition
$AA_{Influx,Base}$	The rate of amino acid influx, in $\frac{amino\ acids}{\Delta t}$, that naïve OT-I T-cells performs
Cyt_0	An integer number representing the number of c-MYC proteins in a naïve OT-I T-cell
$cMYC_{HalfLife}$	The half life, in hours, for individual c-MYC proteins
$cMYC_{Synthesis}$	An integer value for the number of amino acids that assemble to form a single c-MYC protein, in $\frac{cMYC}{amino\ acids}$
$cMYC_{TCR}$	An integer number representing the number of c-MYC proteins produced solely due to TCR stimulation by an APC
$Cyt_{Scaling}$	An integer conversion factor that describes how many additional c-MYC proteins are produced because of additional cytokine output for a given *P*-cell, in $\frac{cMYC}{cytokines}$
MI	The metabolic impairment that is experienced by a $Cell.(\cdot)$ over Δt due to $Acid$ in $\frac{Amino\ Acids}{Lactic\ Acid}$

MP	The metabolic "power" of a single c-MYC molecule, an abstract representation of the many different metabolic pathways that are upregulated by c-MYC
N_{X0}	The total number of cells of type *X* that enter the system boundary.
$p_{A,leave}$	A coefficient used in computing the probability of *A* leaving the system boundary in any given window of size Δt
$p_{AP,Inactivate}$	A coefficient used in computing the probability of an *AP* cell leaving the system boundary in any given window of size Δt
$p_{AB,bind}$	A coefficient used in computing the probability of *A* and *P* binding in any given window of size Δt
$p_{BP,leave}$	A coefficient used in computing the probability of *BP* leaving the system boundary in any given window of size Δt
$p_{EH,leave}$	A coefficient used in computing the probability that an *E*, *F*, *G*, or *H* will leave the system boundary in any given window of size Δt
$p_{IJ,leave}$	A coefficient used in computing the probability that an *I* or *J* will leave the system boundary in any given window of size Δt
$r_{Glyc,Base}$	The glycolytic rate, in $\frac{lactic\ acid}{\Delta t}$, of a naive OT-I T-cell
$r_{Glyc,Max}$	The maximum glycolytic rate of an OT-I T-cell

$\Delta t_{arrival}$	The period of time over which injected cells enter into the system boundary
t_f	The simulation stopping time
t_m	A measure of how many hours are left in mitosis
μ_{Cyt}	A statistical parameter that determines the shape of the lognormal cytokine secretion profile for an individual *P* cell
$\mu_{PActivation}$	A statistical parameter that determines the shape of the normal distribution for *P* cell activation
σ_{Cyt}	A statistical parameter that determines the shape of the lognormal cytokine secretion profile for an individual *P* cell
$\sigma_{PActivation}$	A statistical parameter that determines the shape of the normal distribution for *P* cell activation

Table 3: List of variables computed during the STORE.2 simulation.

Variable	Definition
AA_{Influx}	The number of amino acids fluxed into a single $Cell.(\cdot)$ over a single Δt
$Acid$	The sum of all LA produced over a single Δt
Age	The age of $Cell.(\cdot)$ since its last division, or its creation. Its current age is given as the end of Δt

$Cell.(\cdot)$	An individual cell with the following variables tracked: Age_{Cell}, Age_P, $Class$, $cMYC$, $Daughters$, LA, $p_{P,Arrival}$, $Prog$, r_{Glyc}, $Stage$, t_m,
$Class$	A record of the generation of $Cell.(\cdot)$
$cMYC$	An integer number of c-MYC proteins per $Cell.(\cdot)$
$Cyt, \Delta t$	The integer number of cytokines received by a single $Cell.(\cdot)$
$Daughters$	The integer number of clonal daughter cells produced by the original *A* cell "mother," and as a collective share the characteristics of $Cell.(\cdot)$
$Decayed$	The integer number of c-MYC proteins that have decayed via the half life over Δt for a $Cell.(\cdot)$
$Feedback$	The integer number of c-MYC proteins produced via the c-MYC positive feedback loop over Δt for a $Cell.(\cdot)$
LA	The integer number of lactic acid molecules produced over a Δt for a $Cell.(\cdot)$
$N_{AP,\Delta t}$	The integer number of *AP* cells created per Δt
N_X	The number of cells of type X in the system at any given time
N_{X0}	The total number of cells of type X that enter into the system boundary.
P_{Cyt}	A lognormal distribution, in cytokines versus time, representing the lifetime cytokine secretion profile for *P* cells

$P_{Induced}$	The integer number of c-MYC proteins produced via *P*-cell cytokine-secretions over Δt for a $Cell.(\cdot)$
$P_{P,Act}$	A normal distribution representing all the possible activation times, in hours, for *P* cells
$Prog$	A measure of what percentage of the way the $Cell.(\cdot)$ is to reaching G2/M point from G1 (0-100%)
r_{AP}	The ratio of A entering the system relative to *P* entering the system ($\frac{N_{A0}}{N_{P0}}$)
r_{Glyc}	The glycolytic rate of a $Cell.(\cdot)$ in $\frac{\text{lactic acid}}{\Delta t}$
$Stage$	A record of whether $Cell.(\cdot)$ is mitotic or pre-mitotic
t	The simulation time, in hours.
Δt	The simulation timestep size, in hours.
t_{Act}	The activation time of the bound *P* (if applicable) for $Cell.(\cdot)$
$tot_{AP,Created}$	An integer number of the total number of *AP* cells ever created
X	The set of possible variable cell types, $X = \{AP, BP, C, D, E, F, G, H, I, J, K\}$
δ_1	A binary variable listing whether all cells in the system are or aren't bound to a *P* cell
δ_2	A binary variable listing the mitotic states of all cells in the system

2.2. STORE.2 Overview

The STORE.2 model is a finite state machine that builds upon the STORE.1 model by introducing the c-MYC protein in a quantitative manner, tying its abundance in individual cells to their proliferative ability. The STORE.2 model consequently replaces the STORE.1 probabilistic transitions of one generation to the next. However, it retains many of the surrounding functions that are not affected by c-MYC: the linear arrival of *A* and *P* cells (2.2.2), *A* and *P* binding to form *AP* cells (2.2.5), The *AP* transition to the Nur77^{GFP+} *BP* cells (2.2.6), the *BP* leaving rate (2.2.7), and the *C* through *J* leaving rates (2.2.14). A graphical summary of the STORE.2 model is shown in figure 2, with descriptions of specific functions in chapters 2.2.2 - 2.2.14. For those functions that have been detailed in the previous STORE.1 paper by Christian et al., only summarized descriptions of their relevant methodology will be covered.[1]

The STORE.2 model uses a mixture of stochastic and deterministic functions. It introduces leaving rates for *A* cells (2.2.4), inactivation rates for *AP* cells (2.2.12), *P*-induced c-MYC (2.2.8), c-MYC positive feedback loops (2.2.9), a c-MYC half-life (2.2.10), and a division of the cell cycle into pre-mitotic and mitotic phases (2.2.13). The model does not include death proteins due to insufficient research, hence lower confidence in late-time data post-170 hours.

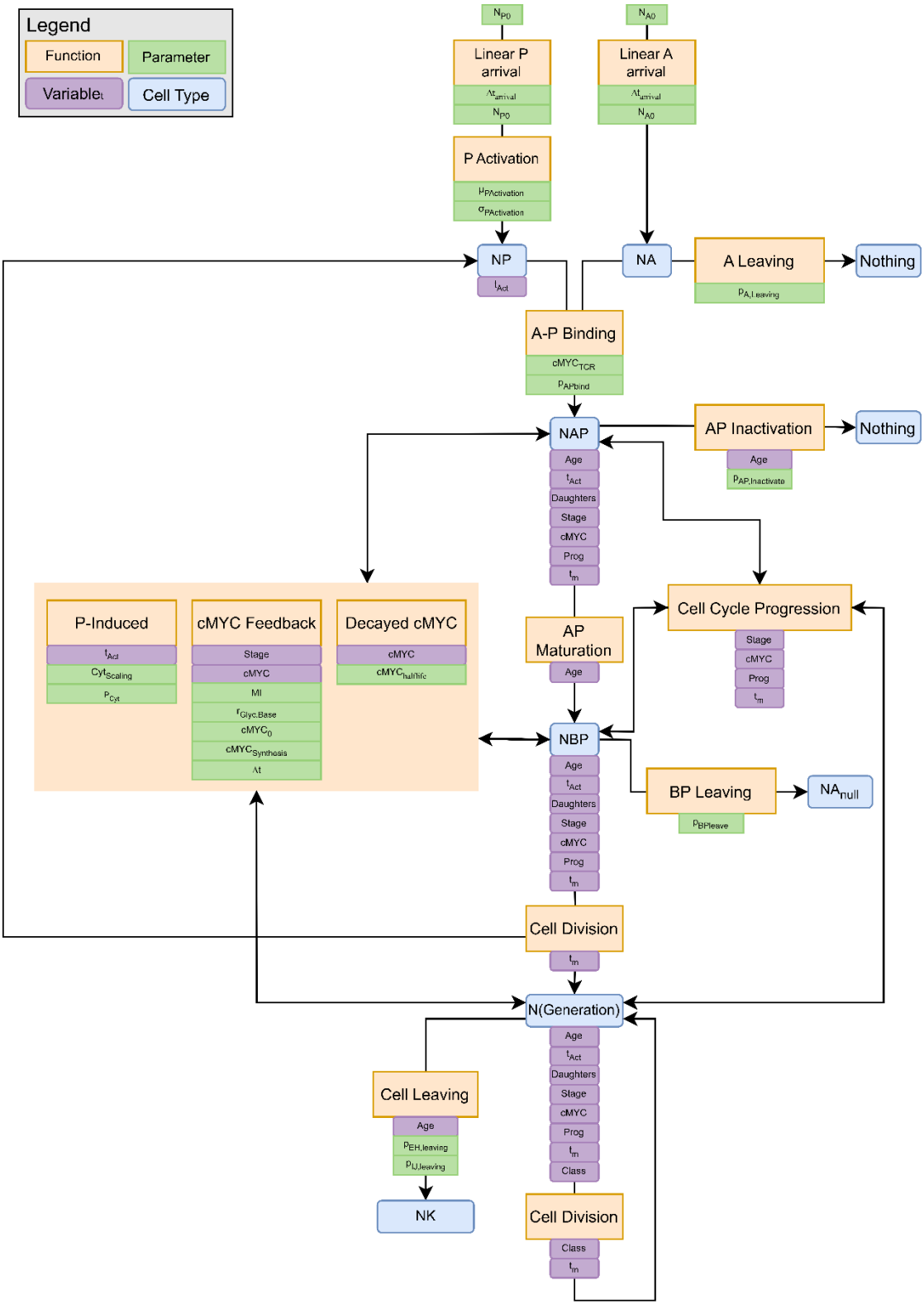

Figure 2: Graphical summary of STORE.2 functions and relevant variables and parameters

2.2.1. System Scope

The boundaries of the model are the parts of the omentum where T cell activation and division occur. *A* and *P* cells enter the system boundary. Cells *AP*, *BP*, and *E-J* can leave the system. Only phenomena inside the system are modelled, including cell division and c-MYC feedback dynamics. Cells outside the system are designated *K* cells and tracked no further.

The simulation start time is the moment the first *A* enters the system. Time is delineated into timesteps of length Δt hours, where Δt = 0.1 hours (6 minutes).

The simulation is considered to reflect immunological reality up to 170 hours, whereupon additional phenomena that are not modelled are expected to influence cell counts. The simulation stop time continues past 170 hours as the resulting dynamics have either been recorded in literature or have implications for improving the model in the future.

2.2.2. Linear arrival of A and P

A and *P* cells arrive in integer amounts each time step at a rate of approximately $\frac{N_{A0}}{\Delta t_{arrival}}$ and $\frac{N_{P0}}{\Delta t_{arrival}}$, respectively. This begins at $t = 0$, and may necessitate multiple *A* and *P* cells arriving in a single Δt. When $t = \Delta t_{arrival}$, $N_{AArrived} = N_{A0}$ and $N_{PArrived} = N_{P0}$. Each time step, an integer number of cells arrive into the system according to equation E1:

(E1) $N_{A,\Delta t} = round((t + \Delta t) \times \frac{N_{A0}}{\Delta t_{arrival}})$

A cells arrive in the system. N_{A0} is the total number of *A* cells injected. $N_{A,\Delta t}$ and $N_{P,\Delta t}$ are the number of *A* and *P* cells that arrive in a given Δt. $N_{AArrived}$ and $N_{PArrived}$ are the number of *A* and *P* cells that have arrived into the system. $\Delta t_{arrival}$ is the span of time over which cells are permitted to enter the system. N_A is a variable that tracks the number of *A* cells in the system. *t* is the current time in the simulation in hours. N_{A0}, N_{P0}, and $\Delta t_{arrival}$ are user-supplied parameters.

2.2.3. Activation of P

In addition to arriving into the system, *P* cells need to activate in order to react with other cells. Each *P* cell activates at a certain time via the probability distribution, $P_{P,Act}$. Activation is probabilistic as in the in vivo experiments, *P* cells activate after the administration of CPS parasites in a stochastic manner that is assumed to be normally distributed The normal distribution is calculated using two parameters: $\mu PActivation$ and $\sigma PActivation$). t_{Act}, the time at which a *P* cell activates will be between:

(E2) $0 \leq t_{Act} \leq \mu PActivation + (3 \times \sigma PActivation)$

The upper bound ensures that all *P* cells are activated by the *T. gondii* parasite before or shortly after they enter the omentum.

2.2.4. A Leaving

A cells continuously circulate throughout the body.[2] To account for this, each timestep, *A* cells will leave the system such that:

(E3) $A \rightarrow (nothing)$

Beginning at $t = 0$, the STORE.2 model uses a user-supplied parameter ($p_{A,leave}$) to determine how many *A* cells leave the system boundary during Δt. The STORE.2 model assumes that *A* cells leave in a linear rate proportional to the rate that they entered the system. The number of *A* cells that leave is determined via equation E4.

(E4) $N_{A,leave} = \left(round\left(p_{AP,leave}(t - \Delta t_{arrival} + \Delta t)\frac{N_{A0}}{\Delta t_{arrival}}\right), N_A\right)$

A leaving occurs after time $\Delta t_{arrival}$. All *A* cells are assumed to be identical, and so they are randomly removed from the count with equal probability, regardless of when they entered the system.

2.2.5. A-P binding

If there are *As* and *Ps* in the system, then every timestep there is a probability for *A-P* binding such that:

(E5) $A + P \rightarrow AP$

$p_{AB,bind}$ is a user-supplied parameter that determines the probability that *P* and *A* cells bind. *NP* is the number of *P* cells in the system. Each Δt there is a chance that any available *A* and *P* cells will bind. The number of *APs* generated in a single Δt is given by equation E6.

(E6) $N_{AP,\Delta t} = p_{AB,bind} \times (\frac{NA}{NA + NP})$

Upon binding and TCR activation, *AP* cells are assigned a $Cell.cMYC$ of $cMYC_{TCR}$. The amount of c-MYC created by TCR activation is assumed to be the same for all cells as each is activated by identical antigen.

2.2.6. AP Maturation

Each timestep, each *AP* has a certain probability that it will mature into *BP*, such that:

(E7) $AP \rightarrow BP$

Each *AP* cell uses a probability distribution function dependent on the *AP*'s age, $Cell.Age_{Cell}$, in hours since it was created, using the beginning of Δt as a reference. *AP* cells transition according to a normal distribution with a standard deviation of 0.15 hours, approximating the maturation time of GFP.[1]

2.2.7. BP Leaving

Each timestep, each *BP* has a certain probability that it will leave the system, such that:

(E8) $BP \rightarrow (nothing)$

Beginning at $t = 0$, the STORE.2 model uses a user-supplied parameter ($p_{BP,leave}$) to determine how many *BP* cells leave the system boundary during Δt. The STORE.2 model assumes that *BP* cells leave in a linear rate proportional to the rate that *P* cells entered the system, as described by equation E9.

(E9) $N_{BP,leave} = \left(round\left(p_{BP,leave}(t - \Delta t_{arrival} + \Delta t)\frac{N_{P0}}{\Delta t_{arrival}}\right), N_{BP}\right)$

BP leaving occurs after time $\Delta t_{arrival}$. All *BP* cells are assumed to be identical, and so they are randomly removed from the count with equal probability, regardless of when they entered the system.

2.2.8. P-Induced c-MYC Increase

When *A* and *B* cells are bound to *P* cells their *Cell.cMYC* increases proportional to the number of cytokines secreted by the *P* cell. Since *P* cell cytokine production over time follows the shape of a skewed pulse, a lognormal distribution serves as a sufficient approximation. The lognormal distribution, P_{Cyt}, is calculated via two user supplied parameters: σ_{Cyt}, and μ_{Cyt}.

In STORE.2, the time since activation for individual P-cells determines how much cytokine they can emit into the tissue of interest. Cytokine secretion is assumed to be a local paracrine phenomenon, experienced by the *A* or *B* cell directly bound to the *P* cell with no residual environmental pool of cytokines. Following *P* cell activation, the cytokine-secretory capacity of a *P* cell increases until it peaks and decays irreversibly. Each *P* cell is assumed to have identical cytokine secretory capacity over its lifetime, though depending on when the *P* cell activates and when it binds to an *A* cell means that each *A* and *B* can receive different cytokine amounts per Δt: cells that activate very early will be at the end of their cytokine pulse by the time they arrive,

whereas cells that activate late will peak around or after the time of arrival into the omentum. Each timestep, *A* and *P* cells receive cytokines according to equation E10.

(E10) $Cell.Cyt, \Delta t \ = \ \delta_1 \ \times \ P_{Cyt}(Cell.Age_P, t, \Delta t)$

δ_1 is a binary variable that determines if a cell in question is bound to a *P* cell. The number of cytokines produced over Δt is calculated by determining how old the *P* cell is, and thus, what are the appropriate cytokines for it to produce. Each *P* cell is considered to be identical save for when each was activated. Once the number of cytokines secreted over the timestep is calculated, it is converted into additional c-MYC molecules via equation E11.

(E11) $Cell.P_{Induced} = round\big(Cyt_{Scaling} \times Cell.Cyt, \Delta t\big)$

$Cyt_{Scaling}$ is a user-provided scalar value of units $\frac{c-MYC}{cytokines}$ that converts the amount of cytokine secreted that Δt into c-MYC. *A* cells that have not been activated by a *P* cell do not have their c-MYC levels augmented, as the T cell receptor is a key switch to begin c-MYC synthesis.[31]

2.2.9. c-MYC Feedback Regulation

c-MYC metabolic upregulation for an individual cell is assumed to be directly proportional to the ratio $\frac{Cell.cMYC}{cMYC_0}$, i.e. the base glycolytic rate of naïve OT-I T cells is augmented by the ratio of the cell's c-MYC in relation to the c-MYC of naïve OT-I T cells. $cMYC_0$ is low, as naïve T cells show almost no c-MYC.[3,4] Each timestep, the model calculates individual glycolytic rates (r_{Glyc}) via equation E12.

(E12) $Cell.r_{Glyc} \ = min\ \left(\frac{r_{Glyc,Base} \times Cell.cMYC}{cMYC_0}, r_{Glyc,Max}\right)$

$Cell.r_{Glyc,Max}$ serves as an upper limit on the glycolytic rate possible for individual OT-I T cells. It is equal to three times the base glycolytic rate.[5,6] Lactic acid is produced as a result of the

glycolytic rate, and subsequently impacts the pH of the system. pH is not directly tracked as the STORE.2 model has no measure of the size of the cellular microenvironment. Instead, the total number of lactic acid molecules produced by all cells in the system over the entire time step serves as a proxy for pH. Individual lactic acid molecules are assumed to not last beyond the six-minute timestep, being a local phenomenon that is buffered by the bicarbonate buffer system. The quantity of lactic acid is calculated via equation E13.

(E13) $Acid \ = \ \Sigma\big(Cell.r_{Glyc} \times Cell.Daughters \ \times \ \Delta t\big)$

Each timestep, AA_{Influx}, just like the glycolytic rate, is augmented by the $\frac{Cell.cMYC}{cMYC_0}$ ratio, however, it is further affected by the quantity of $Acid$. $Acid$ impairs the c-MYC-augmented amino acid influx rate via the scalar multiplier MI, which is measured in terms of $\frac{amino\ acids}{lactic\ acids}$, as can be seen in equation E14.

(E14) $Cell.AA_{Influx} \ = \left(\frac{AA_{Influx,Base} \times Cell.cMYC}{cMYC_0} - (MI \times Acid)\right) \times \Delta t$

Amino acids are converted into c-MYC proteins via the $cMYC_{Synthesis}$. The only cells that are subject to c-MYC positive feedback are pre-mitotic cells, which are accounted by the binary variable, δ_2. c-MYC for individual cells are then calculated via E15.

(E15) $Cell.Feedback \ = \ round\big(Cell.\delta_2 \ \times cMYC_{Synthesis} \ \times \ Cell.Cell.AA_{Influx}\big)$

δ_2 is a conditional array of cells that are pre-mitotic. The amino acids brought into the cell are then converted into c-MYC via a scalar multiplier. c-MYC dynamics over the course of the cell cycle are simplified such that c-MYC feedback occurs only during G1-G2, and that the parameters that govern feedback do not change over the course of the cell cycle. It is done this way as there is insufficient evidence for c-MYC dynamics changing over the course of G1-G2.

2.2.10. c-MYC Decay

Regardless of simulation time, cell generation, or mitotic state, each timestep, all c-MYC is subject to decay. Each Δt, a cell's c-MYC decays according to a user-supplied half-life. The c-MYC half-life was found in literature, though the nuances of c-MYC decay via c-MYC stabilization and enzymatic degradation dynamics are not fully explored due to insufficient data in many key protein levels.

(E16) $$Cell.Decayed = round\left(Cell.cMYC - (1 - 0.5^{\frac{\Delta t}{cMYC_{HalfLife}}}) \right)$$

2.2.11. c-MYC Summation

Each timestep, the result of each of the three c-MYC-influencing dynamics are summed to determine the new, unique c-MYC total for each cell.

(E17) $$Cell.cMYC = Cell.cMYC + Cell.PInduced + Cell.Feedback + Cell.Decayed)$$

2.2.12. AP Inactivation

Due to the probabilistic nature of the *AP*-*BP* transition, a handful of *AP* cells will remain in the *AP* state in perpetuity. These cells exponentially increase their c-MYC levels as no cell division occurs to halve/decay their c-MYC quantity. Since only *BPs* can transition into *Cs*, these c-MYC rich *APs* represent a clear anomaly. To prevent them from skewing average c-MYC counts for all the remaining *A* cells, an *AP* inactivation probability is introduced to the STORE.2 model to represent that the cells that fail to transition to *BPs* enter a period of quiescence similar to the G0 state of inactive naive *A* cells.

Each timestep, each *AP* has a certain probability that it will inactivate, such that:

(E19) $$AP \rightarrow (nothing)$$

Each *AP* cell uses the $p_{AP,Inactivate}$ probability distribution function to determine when it will transition. *AP* cells with an older $Cell.Age_{Cell}$ are more likely to transition. $p_{AP,Inactivate}$ is a normal distribution with a standard deviation of approximately two hours, and a minimum inactivation time of 1.5 hours, beyond when an *AP* should have transitioned to a *BP*.

2.2.13. Cell cycle progression

Each timestep, individual cells are checked for whether they are pre-mitotic or mitotic, the value of which is recorded by $Cell.Stage$. If the cell is pre-mitotic then its metabolic progress towards the G2/M checkpoint as stored in the $Cell.Progress$ variable is evaluated. If the cell is 100% towards completing the metabolic upregulation needed to pass the G2/M checkpoint then the $Cell.Stage$ is changed to reflect that the cell is now mitotic, and the t_m is set to one hour. If $Cell.Progress$ does not reflect 100% metabolic advancement towards the G2/M restriction point, then it is increased according to equation E20.

(E20) $Cell.Progress = MP \times Cell.cMYC$

Each c-MYC protein in the cell is assumed to be equally capable of advancing the necessary metabolic pathways that enable the cell to prepare for mitosis, with each c-MYC protein increasing $Cell.Progress$ by the scalar multiplier, MP.

If a cell is mitotic, then its $Cell.t_m$ will be evaluated to see if it is negative, or equal to 0 hours. t_m, the length of M-phase, is held constant throughout the simulation as there is insufficient evidence of c-MYC augmenting the length of the mitotic phase. If not, then the cell has not completed mitosis and a new $Cell.t_m$ is calculated via equation E21.

(E21) $Cell.t_m = Cell.t_m - \Delta t$

If $Cell.t_m$ is less than or equal to 0 hours, then the cell is considered to have completed mitosis and the following changes occur to $Cell$:

Table 4: Changes to cell variables following mitosis completion.

Class	The cell progresses to the next generation, i.e. *C* to *D*. If the cell is a *J* then the cell remains a *J* cell as the *J* class encapsulate all daughters of a *J* cell.
Stage	The stage is changed to be pre-mitotic.
Progress	Metabolic progress towards G2/M restriction point is reset to 0%.
Age_{Cell}	The age of the cell is reset to 0 hours.
Daughters	The total number of cells represented by this specific *Cell.Class*, *Cell.Stage*, *Cell.Progress*, *Cell.Age* is duplicated.

2.2.14. Cell leaving rates

Each timestep, each *Cell* of $Cell.Class \geq 5$ (E-J) has a certain probability that it will leave the system, before it divides, whereupon it is classified as type *K*, according to the following transitions:

(E22) $E \rightarrow K$

(E23) $F \rightarrow K$

(E24) $G \rightarrow K$

(E25) $H \rightarrow K$

(E26) $I \rightarrow K$

(E27) $J \rightarrow K$

Cells *E-H* have a user-supplied probability of leaving ($P_{EH}, leave$) and cells *I-J* have a different user-supplied probability of leaving ($P_{IJ}, leave$).

2.3. Parameter Estimation

The STORE.2 model introduced new parameters into the model that, while representing the current conception of c-MYC dynamics during $CD8^+$ proliferation, lack explicit values. To determine the value of these parameters for the STORE.2 model, an optimization framework based on *in vivo* mouse data was used.

2.3.1. In Vivo Data

The reference data for optimization were cell counts of fluorescent ovalbumin-specific CD8+ (OT-I) T cells transferred intraperitoneally into wild-type (WT) and $Batf3^{-/-}$ mice (KO) that were subsequently vaccinated intraperitoneally 2 hours later with the CPS strain of the parasite *Toxoplasma gondii* as reported by Christian et al.[1] 4-5 mice were sacrificed and had their T-cells harvested for each selected time point (Table). Since each mouse represented a single measurement of a single time point, mouse cell counts were averaged and collected to generate "composite" mice.[1]

Table 5: WT composite mice cell counts and standard error of the mean.

	WT Composite Mouse Cell Count Averages					WT Composite Mouse standard error of the mean				
Day	2	3	4	6	8	2	3	4	6	8
A	3326	1298	1815	667	280	1292	1241	749	372	63.2
BP	970	882	496	258	33	358	813	173	112	23.5

C	134	917	603	338	146	48	859	272	150	43.3
D	81	1516	791	586	220	45	1401	308	280	47.3
E	47	2223	1360	810	470	30	1979	550	362	106.9
F	15	2940	2242	1276	686	6	2585	904	387	207.3
G	1	3172	3643	1697	972	1	2712	1478	427	307.0
H	1	2804	4228	2046	1084	1	2277	1714	407	295.5
I	0	1989	4812	2634	1073	0	1556	1964	464	312.0
J	2	738	15415	153004	111515	1	584	5222	28295	32399.3
Time (hr)	30	68	92	140	188	30	68	92	140	188

Table 6: KO composite mice cell counts and standard error of the mean.

	KO Composite Mouse Cell Count Averages					KO Composite Mouse standard error of the mean				
Day	2	3	4	6	8	2	3	4	6	8
A	3145	1770	942	4925	280	1690.4	916	432	1896	63
BP	981	718	445	1206	33	703.0	335	225	345	24
C	344	215	191	1169	146	194.7	100	114	380	43
D	276	176	227	1186	220	173.3	65	133	312	47
E	190	196	375	1306	470	115.3	76	233	327	107
F	49	208	440	1424	686	36.3	49	275	369	207
G	2	176	533	1512	972	1.8	35	303	329	307

H	1	142	520	1423	1084	0.8	35	298	348	296
I	1	94	638	1793	1073	0.8	19	372	509	312
J	1	21	1954	50484	111515	0.8	8	1172	15643	32399
Time (hr)	30	68	92	140	188	30	68	92	140	188

2.3.2. Difference between WT and KO

Previous work showed that OT-I T cells activated in CPS-immunized Batf3$^{-/-}$ mice showed lower expression levels for CD71, CD98, and CD25 the OT-I T cells from WT mice. CD71 is a Transferrin receptor that enables cellular iron uptake via binding to the iron carrier, transferrin.[7] CD98 enables clonal expansion by amplifying pro-proliferation and anti-apoptotic integrin signals.[8] CD98 is also a type 2 transmembrane protein (specifically part of the SLC3A amino acid transporter) that covalently links to L-type amino acid transporters (which transport large neutral amino acids) such as SLC7A5.[9,10] Finally, CD25 is the IL-2 receptor-α; IL-2 influences CD8+ T cell proliferation and differentiation, enabling the production of IFN-γ, TNF-α, and lymphotoxin α, as well as enabling several killing-mechanisms such as perforins and granzymes.[11]

To represent the deficiencies in cell metabolism, OT-I T cells from immunized *Batf3*$^{-/-}$ mice were expected to have lower MP than cells from WT mice. Transcriptomic analyses have shown that c-MYC binding targets are upregulated to a higher degree in activated OT-I cells from WT mice than those from Batf3$^{-/-}$ mice [unpublished data].

2.3.3. The Optimization Problem

The model was fit to the composite mouse data by solving the following stochastic optimization equations:

(E28) $\underline{E_A} = \underline{N_A} - \underline{Y_A}$

(E29) $\underline{E_{BP}} = \underline{N_{BP}} - \underline{Y_{BP}}$

(E30) $\underline{E_C} = \underline{N_C} - \underline{Y_C}$

(E31) $\underline{E_D} = \underline{N_D} - \underline{Y_D}$

…

(E32) $\underline{E_I} = \underline{N_I} - \underline{Y_I}$

(E33) $OF_A = \|\underline{E_A}\|$

(E34) $OF_{BP} = \|\underline{E_{BP}}\|$

(E35) $OF_{CH} = \frac{1}{\sqrt{6}}\|\frac{\underline{E_C}}{2}, \frac{\underline{E_D}}{4}, \frac{\underline{E_E}}{8}, \frac{\underline{E_F}}{16}, \frac{\underline{E_G}}{32}, \frac{\underline{E_H}}{64}\|$

(E36) $OF_I = \|\frac{\underline{E_I}}{128}\|$

(E37) $OF = min(OF_A + OF_{BP} + OF_{EH} + OF_I)$

Table 7: Upper and lower bounds of the search space for STORE.2 optimization parameters

Parameter	Lower Bound	Upper bound
$AA_{Influx,Base}$	10^2	10^3
$cMYC_0$	1	50
$cMYC_{HalfLife}$	Fixed due to estimates of the AP4 half life of 2.5 hours.[12]	

$cMYC_{Synthesis}$	Fixed due to the constant size of the c-MYC protein of 437 amino acids.[13]	
$Cyt_{Scaling}$	10^0	10^3
Cyt_{TCR}	Fixed at 2000 c-MYC proteins due to c-MYC quantification in AP cells [unpublished data].	
MI	10^{-8}	10^{-4}
MP	10^{-8}	10^{-4}
$p_{AP,Inactivate}$	0	1
$p_{A,leave}$	0	1
$r_{Glyc,Base}$	10^1	10^3
t_m	Fixed at 1 hour due to literature estimates of cell cycle lengths.[14]	
μ_{Cyt}	0	5
$\mu_{PActivation}$	10	17
σ_{Cyt}	0	1
$\sigma_{PActivation}$	0	5

$\underline{E_X}$ are the errors for a cell of type X, representing the deviation between model cell counts ($\underline{N_X}$) and data cell counts ($\underline{Y_X}$). Both ($\underline{N_X}$) and ($\underline{Y_X}$) are collections of cell counts at harvest time points. $\underline{E_X}$ is scaled according to the generation of X to account for the fact that with each division, the cell count effectively doubles. If $\underline{E_X}$ was not scaled, then later generations would exert outsized influence on subsequent calculations.

Different cell generations are segregated into four groups: *A*, *BP*, *C-H*, and *I*, with each group having the same relative weight on the total objective function. Cells within a group follow similar behaviour, for example, *E* cell leaving rates, counts, and behaviour correlate strongly with *F* cells, while being significantly different from *A* cells.

OF, or objective function, values for different cell types are calculated via the euclidean norm of the scaled errors. Geometrically, $\underline{N_X}$ and $\underline{Y_X}$ are coordinates on a euclidean plane, where OF_X is the distance between them.

Finally, the dividing of *E-H* by √6 accounts for the number of cell types considered within each group such that they are equally weighted with the same relative importance during parameter estimation. The *J* cell count is not considered for optimization because the rate of cell division varies over time for each individual cell based on its unique c-MYC count. Since *J* cells can generate 2 new *J* cells at an unknown variable rate in the STORE.2 model, a scaling factor cannot be used.

2.3.4. Particle Swarm Optimization

The model underwent particle swarm optimization, whereby virtual particles explore the multidimensional space that represents all possible parameter values, seeking a combination of

values that result in minimal deviation of experimental and simulated data. The key optimization equation the model seeks to minimize is equation E37.

Optimization was carried out on a Dell XPS 13 (790) laptop with a 10th generation intel processor. Parameters optimized in the previous STORE.1 model were not changed, as functions regarding cell arrival, leaving, binding, and expression of Nur77^{GFP+} should not be affected by the introduction of c-MYC.

Each session of optimization used 50 virtual particles for 100 rounds of optimization. With a single session of optimization that could take 12-24 hours to run, to speed up computation, a parallel pool of virtual workers was set up, allowing the particle swarm optimization to be run in parallel. 4 workers, one per physical CPU core were used. The final parameters determined after 50 rounds of optimization are as follows:

Table 8: Final STORE.2 parameters after 50 rounds of optimization

Parameter	WT-Residing Cell Value	KO-Residing Cell Value
$AA_{Influx,Base}$	$10^{2.2285}$	$10^{2.2285}$
$cMYC_{HalfLife}$	2.5	2.5
$cMYC_0$	10	10
$cMYC_{Synthesis}$	439	439
$Cyt_{Scaling}$	$10^{1.5451}$	$10^{1.5451}$
Cyt_{TCR}	2000	2000
MI	$10^{-6.0083}$	$10^{-6.0083}$

MP	$10^{-5.9636}$	$10^{-6.5304}$
$p_{AP,Inactivate}$	0.20	0.010
$p_{A,leave}$	0.030	0.080
$r_{Glyc,Base}$	10^2	10^2
t_m	1	1
μ_{Cyt}	2	2
$\mu_{PActivation}$	12.94	12.94
σ_{Cyt}	0.40	0.40
$\sigma_{PActivation}$	3	3

2.4. References

1) Christian, David A, Thomas A Adams, Lindsey Shallberg, Anthony T Phan, Tony E Smith, Mosana Abraha, Joseph W Perry, et al. “CDC1 Coordinate Innate and Adaptive Responses in the Omentum Required for T Cell Priming and Memory.” *Science Immunology* 7, no. 75 (September 30, 2022). https://doi.org/10.1126/sciimmunol.abq7432.
2) Mandl, Judith N., Rachel Liou, Frederick Klauschen, Nienke Vrisekoop, João P. Monteiro, Andrew J. Yates, Alex Y. Huang, and Ronald N. Germain. “Quantification of Lymph Node Transit Times Reveals Differences in Antigen Surveillance Strategies of Naïve CD4+ and CD8+ T Cells.” *Proceedings of the National Academy of Sciences* 109, no. 44 (October 30, 2012): 18036–41. https://doi.org/10.1073/pnas.1211717109.

3) Preston, Gavin C, Linda V Sinclair, Aneesa Kaskar, Jens L Hukelmann, Maria N Navarro, Isabel Ferrero, H Robson MacDonald, Victoria H Cowling, and Doreen A Cantrell. “Single Cell Tuning of Myc Expression by Antigen Receptor Signal Strength and Interleukin-2 in T Lymphocytes.” *The EMBO Journal* 34, no. 15 (July 2015): 2008–24. https://doi.org/10.15252/embj.201490252.
4) Gnanaprakasam, J.N. Rashida, and Ruoning Wang. “MYC in Regulating Immunity: Metabolism and Beyond.” *Genes* 8, no. 3 (February 24, 2017): 88. https://doi.org/10.3390/genes8030088.
5) Quinn, Kylie M., Tabinda Hussain, Felix Kraus, Luke E. Formosa, Wai K. Lam, Michael J. Dagley, Eleanor C. Saunders, et al. “Metabolic Characteristics of CD8+ T Cell Subsets in Young and Aged Individuals Are Not Predictive of Functionality.” *Nature Communications* 11, no. 1 (June 5, 2020): 2857. https://doi.org/10.1038/s41467-020-16633-7.
6) Jones, Nicholas, James G Cronin, Garry Dolton, Silvia Panetti, Andrea, Sarah, Andrew K Sewell, David K Cole, Catherine A Thornton, and Nigel J Francis. “Metabolic Adaptation of Human CD4+ and CD8+ T-Cells to T-Cell Receptor-Mediated Stimulation.” *Frontiers in Immunology* 8 (November 9, 2017). https://doi.org/10.3389/fimmu.2017.01516.
7) Guo, Zilong, Yirui Zhang, Mingpeng Fu, Liang Zhao, Zhen Wang, Zhuoshuo Xu, Huifen Zhu, et al. “The Transferrin Receptor-Directed CAR for the Therapy of Hematologic Malignancies.” *Frontiers in Immunology* 12 (March 29, 2021). https://doi.org/10.3389/fimmu.2021.652924.
8) Cantor, J. M., and M. H. Ginsberg. “CD98 at the Crossroads of Adaptive Immunity and Cancer.” *Journal of Cell Science* 125, no. 6 (March 15, 2012): 1373–82. https://doi.org/10.1242/jcs.096040.
9) Nguyen, Hang Thi Thu, and Didier Merlin. “Homeostatic and Innate Immune Responses: Role of the Transmembrane Glycoprotein CD98.” *Cellular and Molecular Life Sciences* 69, no. 18 (March 30, 2012): 3015–26. https://doi.org/10.1007/s00018-012-0963-z.
10) Ross, Sarah H, and Doreen A Cantrell. “Signaling and Function of Interleukin-2 in T Lymphocytes.” *Annual Review of Immunology* 36 (2018): 411–33. https://doi.org/10.1146/annurev-immunol-042617-053352.
11) Cheng, Hongcheng, Yajing Qiu, Yue Xu, Lan Chen, Kaili Ma, Mengyuan Tao, Luke Frankiw, et al. “Extracellular Acidosis Restricts One-Carbon Metabolism and Preserves T Cell

Stemness." *Nature Metabolism* 5, no. 2 (January 30, 2023): 314–30. https://doi.org/10.1038/s42255-022-00730-6.

12) Chou, Chun, Amelia K. Pinto, Jonathan D. Curtis, Stephen P. Persaud, Marina Cella, Chih-Chung Lin, Brian T. Edelson, et al. "C-Myc-Induced Transcription Factor AP4 Is Required for Host Protection Mediated by CD8+ T Cells." *Nature Immunology* 15, no. 9 (September 1, 2014): 884–93. https://doi.org/10.1038/ni.2943.
13) MYC MYC proto-oncogene, bHLH transcription factor [Homo sapiens (human)] [Internet]. Bethesda (MD): National Library of Medicine (US), National Center for Biotechnology Information; 2004 – [cited 2023 12 03]. Available from: https://www.ncbi.nlm.nih.gov/gene/4609
14) Cooper, Geoffrey M. "The Eukaryotic Cell Cycle." *The Cell: A Molecular Approach. 2nd Edition*, 2000. https://www.ncbi.nlm.nih.gov/books/NBK9876/#:~:text=For%20a%20typical%20rapidly%20proliferating.

Chapter 3: Cell Counts

One of the basic aims of the STORE.2 model was to accurately simulate WT and KO resident OT-I T-cell population data using a novel modelled mechanism of cell division. This chapter examines where the STORE.2 model was able to replicate the cell population dynamics of the STORE.1 model, and where the two models diverge.

3.1. Similar and Novel STORE.2 Model Cell Count Dynamics

Visually, STORE.2 cell counts share overarching population dynamics with STORE.1 simulated data (Fig 3). WT cell counts in both models are higher than their corresponding KO cell counts. Both WT and KO cell counts for generations *C* to *I* oscillate and trend downwards. WT cells have higher counts than previous generations as a combination of cell doubling and the rate of cell division stave off cell leaving rates. KO cells by comparison do not exceed the cell count of KO *A* cells until the appearance of KO *J* cells.

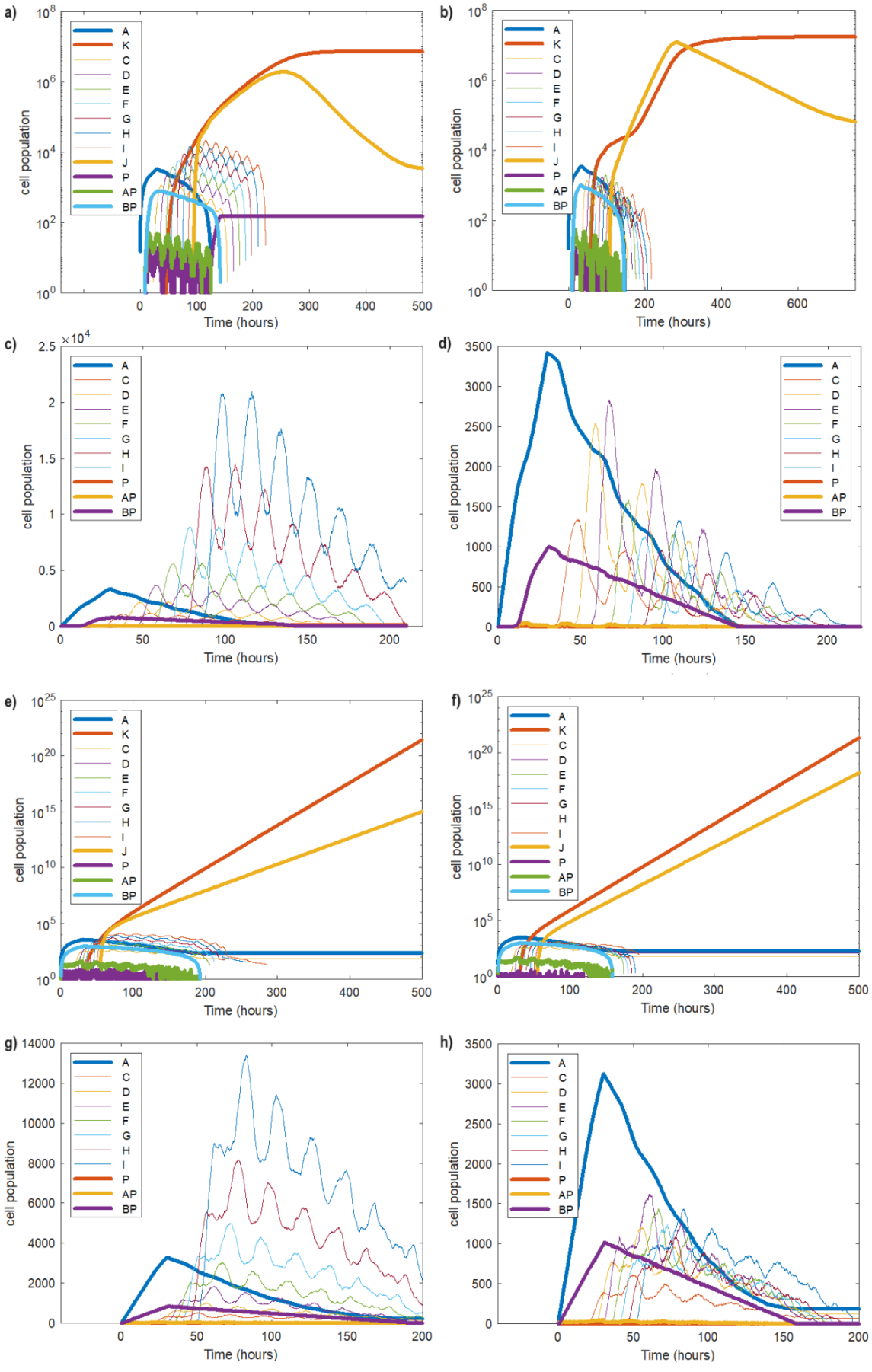
a)
b)
c)
d)
e)
f)
g)
h)
cell population
Time (hours)
A
K
C
D
E
F
G
H
I
J
P
AP
BP

Figure 3: Overall cell counts for WT and KO residing cells in the STORE.1 and STORE.2 models.

a) a STORE.2 simulation of the number of WT OT-I T-cells in divisions 1-8+ versus time

b) a STORE.2 simulation of the number of KO OT-I T-cells in divisions 1-8+ versus time

c) a STORE.2 simulation of the number of WT OT-I T-cells in divisions 1-7 versus time

d) a STORE.2 simulation of the number of KO OT-I T-cells in divisions 1-7 versus time

e) a STORE.1 simulation of the number of WT OT-I T-cells in divisions 1-8+ versus time

f) a STORE.1 simulation of the number of KO OT-I T-cells in divisions 1-8+ versus time

g) a STORE.1 simulation of the number of WT OT-I T-cells in divisions 1-7 versus time

h). a STORE.1 simulation of the number of KO OT-I T-cells in divisions 1-7 versus time

It is with these *J* cell counts for both WT and KO cells that the STORE.2 model significantly diverges from the STORE.1 model. STORE.1 *Js* and *Ks* grow exponentially, while the STORE.2 *Js* irreversibly decline after a period of growth and *K* cell counts effectively plateau, growing modestly, but far below the log-fold increases seen in the STORE.1 model. The result is that the STORE.1 simulations produce final overall cell counts that are several orders of magnitude greater than STORE.2 simulation cell counts. This is to be expected because of a combination of natural cell leaving and the STORE.2 model's emergent mechanism for division cessation. The accumulation of cells in the system produces high volumes of lactic acid (Fig 14), resulting in acid-induced c-MYC feedback inhibition (Fig. 1). Thus, later generations of STORE.2 WT and KO cells are unable to accumulate the necessary c-MYC as fast as they could when overall cell populations were lower, resulting in longer cell cycle durations (Fig. 16). Without c-MYC feedback, c-MYC degradation proceeds unopposed, with c-MYC counts becoming so low that no further cell division is possible.

The STORE.2 model is able to accurately simulate in vivo data on CD8+ T cell clonal expansion up to 170 hours for WT and KO cells. STORE.2 cell counts further than 250 hours show cell counts in the system declining; literature demonstrates that cell counts decline at later time points is expected, though in vivo data for this particular mouse system is lacking.[1] Furthermore, there are phenomena that are excluded that limit cell count accuracy post 170 hours (Chapter 6).

3.2. Generational Differences in Cell Count Between STORE.1 and STORE.2

While STORE.1 and STORE.2 cell counts follow similar general trends for *A* to *I* generations, there are differences in the pattern of cell count fluctuations. The peaks and troughs of these fluctuations create “cohorts” of cells that display similar behaviours over time.

For example, the STORE.2 WT *F* cell counts in Fig. 4c oscillate to form 7 peaks and troughs. The cells in each peak form a cohort.

By comparing differences in the size and distribution of these cohorts in the following plots, nuances of the STORE.1 and STORE.2 model can be examined. Cells of different generations are clustered together for legibility, and normalized cell count values (the cell counts are divided by the corresponding power of 2 to acknowledge that cell count doubles with division) are provided to show the effect that cell leaving has on overall cell counts.

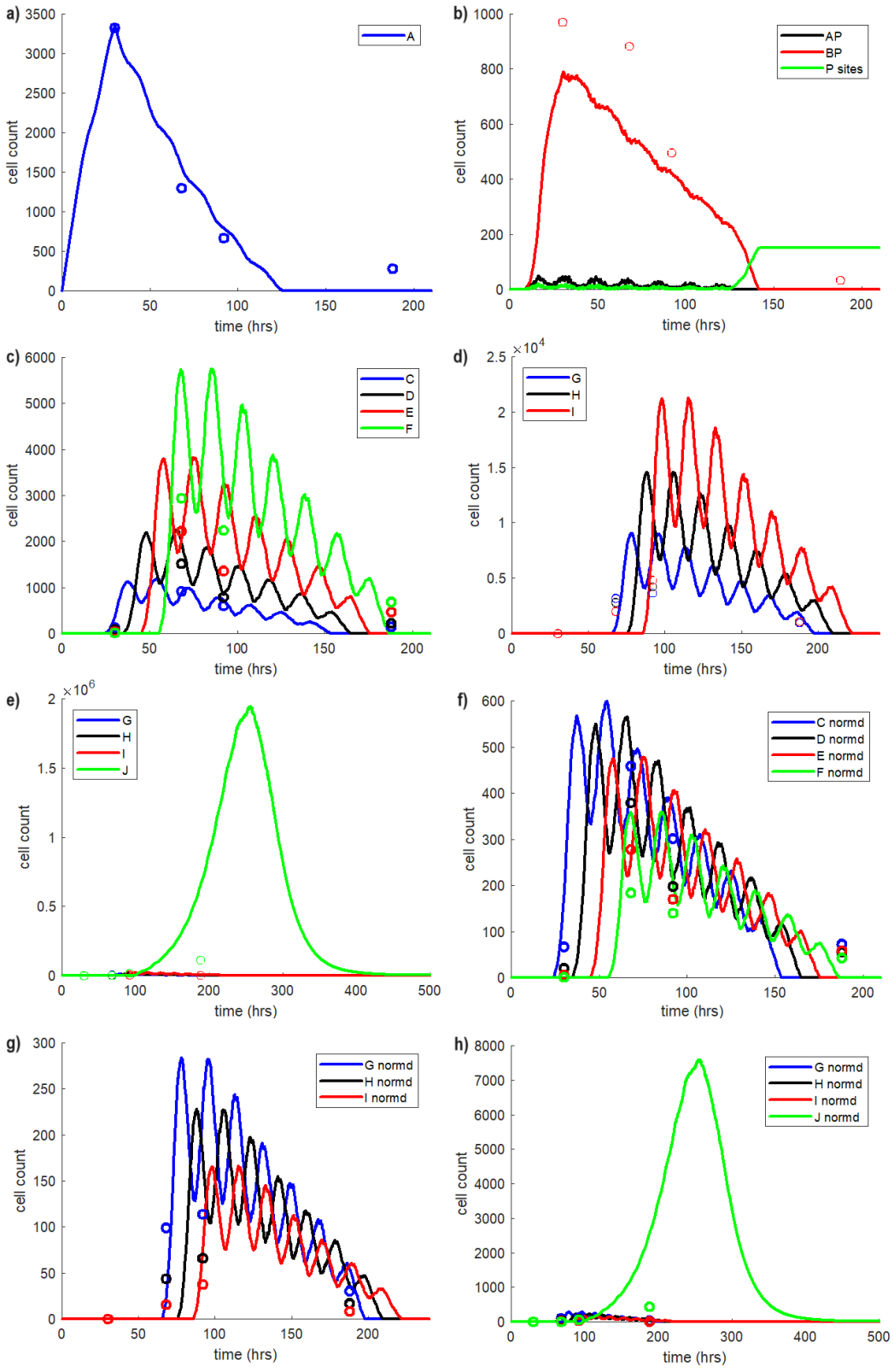

Figure 4: STORE.2 WT cell counts by generation.

a) *Cell counts over time for naïve OT-I T cells.*

b) *Cell counts over time for unbound APCs, APCs bound to Nur77^{GFP-} OT-I T-cells (AP), and APCs bound to Nur77^{GFP+} OT-I T cells (BP).*

c) *Cell counts over time for OT-I T cells that have undergone 1-4 divisions.*

d) *Cell counts over time for OT-I T cells that have undergone 5-7 divisions.*

e) *Cell counts over time for OT-I T cells that have undergone 5-8+ divisions.*

f) *Cell counts over time for OT-I T cells that have undergone 1-4 divisions, scaled according to generation.*

g) *Cell counts over time for OT-I T cells that have undergone 5-7 divisions, scaled according to generation.*

h) *Cell counts over time for OT-I T cells that have undergone 5-8+ divisions, scaled according to generation.*

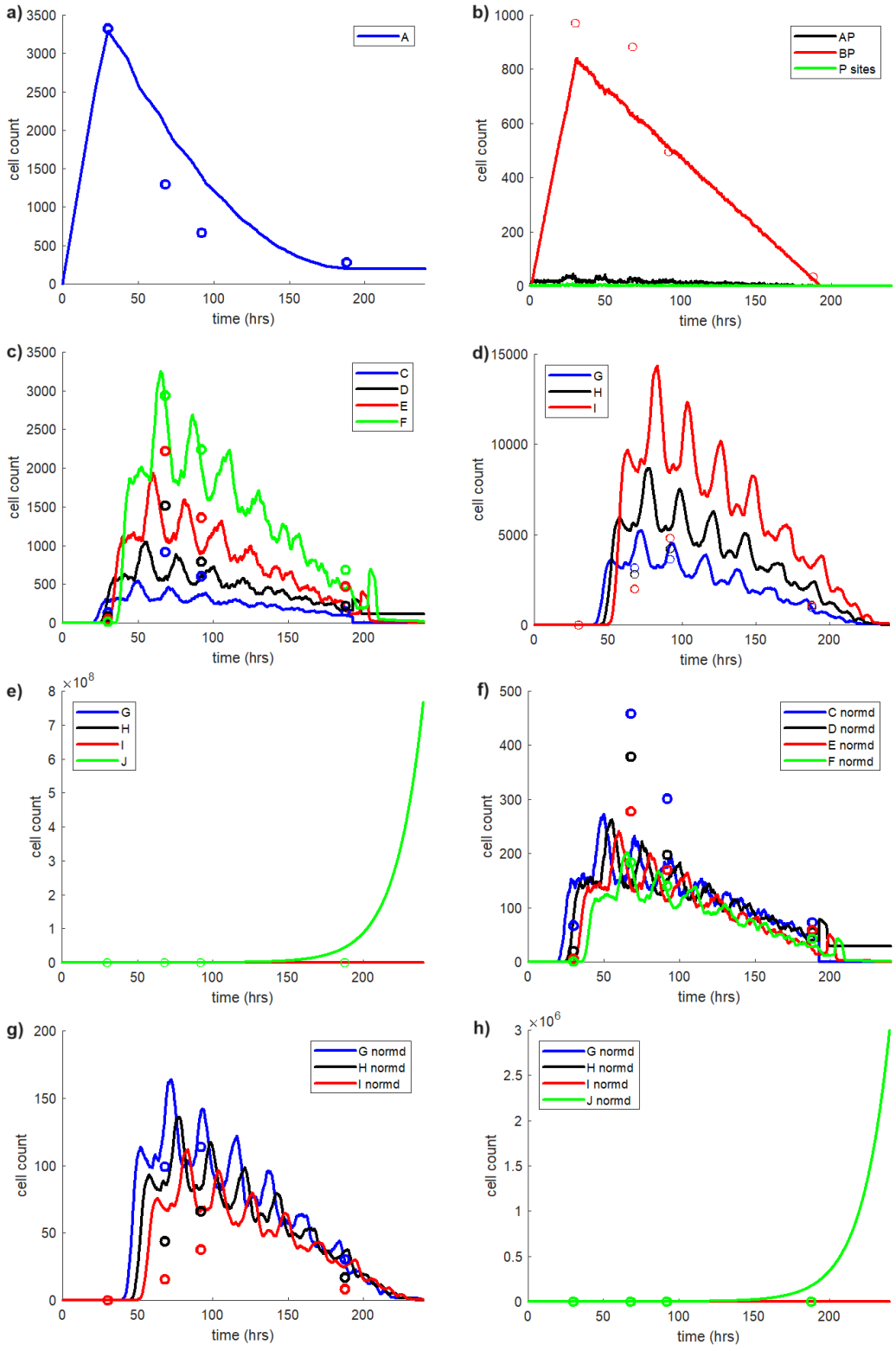

Figure 5: STORE.1 WT cell counts by generation.

a) Cell counts over time for naïve OT-I T cells.

b) *Cell counts over time for unbound APCs, APCs bound to Nur77^{GFP-} OT-I T-cells (AP), and APCs bound to Nur77^{GFP+} OT-I T cells (BP).*

c) *Cell counts over time for OT-I T cells that have undergone 1-4 divisions.*

d) *Cell counts over time for OT-I T cells that have undergone 5-7 divisions.*

e) *Cell counts over time for OT-I T cells that have undergone 5-8+ divisions.*

f) *Cell counts over time for OT-I T cells that have undergone 1-4 divisions, scaled according to generation.*

g) *Cell counts over time for OT-I T cells that have undergone 5-7 divisions, scaled according to generation.*

h) *Cell counts over time for OT-I T cells that have undergone 5-8+ divisions, scaled according to generation.*

STORE.2 WT cell counts are greater than STORE.1 WT cell counts for generations *C* to *I*. This is because STORE.2 WT cells take longer to transition from one generation to the next than STORE.1 WT cells. The slower transition causes cells to remain in their current generation, driving up the corresponding cell count, for example, *C* cells remain as *C* cells long enough that hundreds of *BPs* are able to transition into *Cs*, causing the initial STORE.2 *C* count to grow to approximately 1000 cells by 50 hours (Fig. 4c), while STORE.1 *C* cells are only at approximately 500 cells (Fig. 5c). The slower division time also means that generations of cells appear later in the STORE.2 model than STORE.1. In STORE.1, the cohort of *D* cells appears approximately 5 hours after the first *C* cell cohort appears (the STORE.1 cell generation transition probability is based around a 5.3-hour transition time). In STORE.2, cell cohorts appear approximately 10 hours after the first cohort appearance of their previous generation (Fig. 16). The greater cell counts and spread-out

cohorts of the STORE.2 model leads to improved in vivo data fitting (Chapter 3.4), as can be seen in the normalized cell counts for STORE.1 and STORE.2 simulations, with the former having early cell generations undershooting, and later time points overshooting, in vivo data points.

Additionally, STORE.1 cells form cohorts that are more strongly delineated, whereas the cohort structure in STORE.2 cells are more jagged and appear to break down at later time points. Despite this, the cohort structure appears to originate with earlier generations, as can be seen in the overall visual similarity of different generations of cell count curves in the normalized graphs (Fig. 4f-h); if one knew the shape of the cell counts for the *C* generation, one could easily predict the shapes of generations *D* through *I*. This suggests that the differences in the shapes of STORE.1 and STORE.2 cell counts originate in early generations.

All of these dynamics occur with KO cells as well, as can be seen in the following plots.

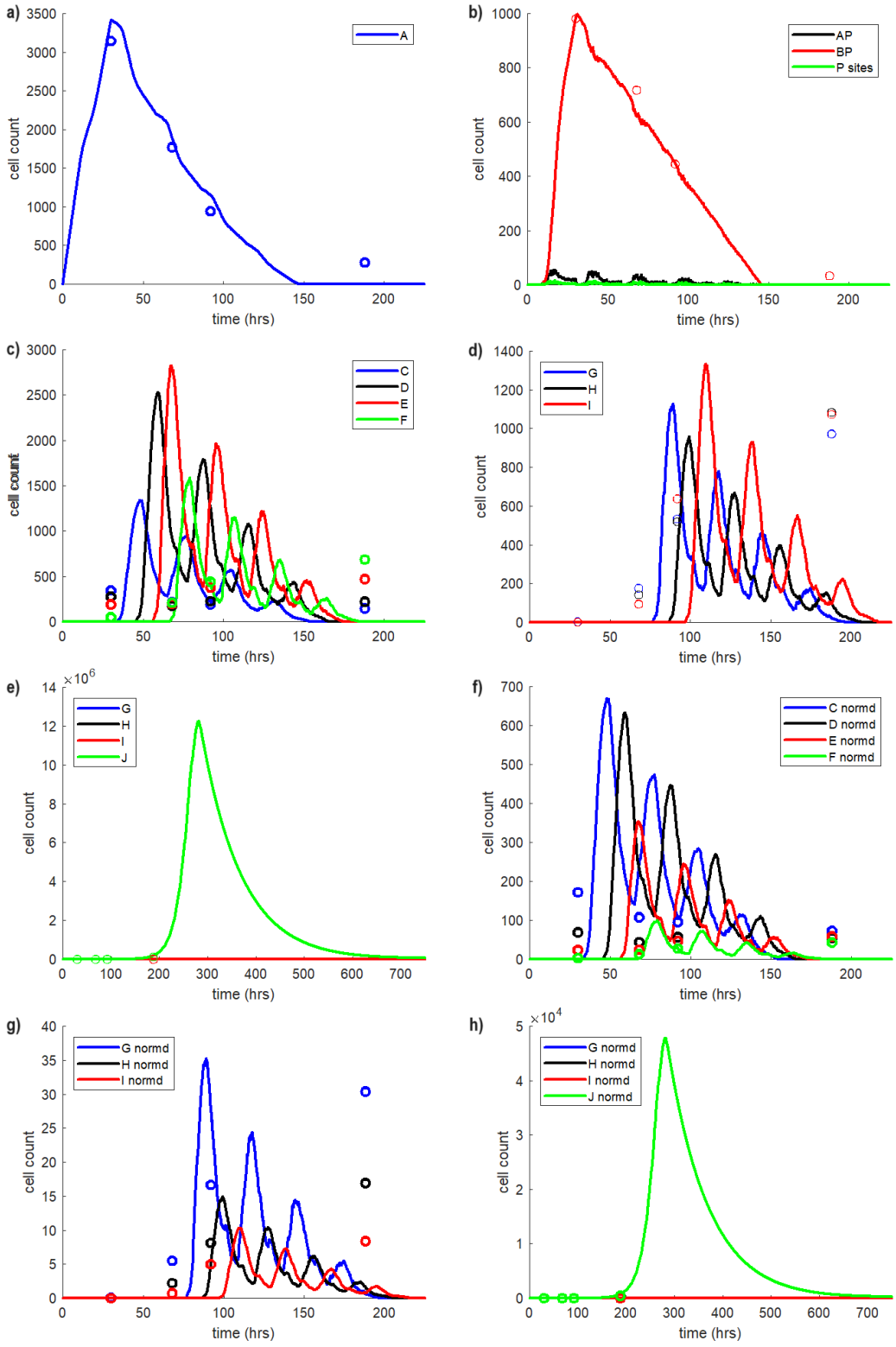

Figure 6: STORE.2 KO cell counts by generation.

a) Cell counts over time for naïve OT-I T cells.

b) *Cell counts over time for unbound APCs, APCs bound to Nur77^{GFP-} OT-I T-cells (AP), and APCs bound to Nur77^{GFP+} OT-I T cells (BP).*

c) *Cell counts over time for OT-I T cells that have undergone 1-4 divisions.*

d) *Cell counts over time for OT-I T cells that have undergone 5-7 divisions.*

e) *Cell counts over time for OT-I T cells that have undergone 5-8+ divisions.*

f) *Cell counts over time for OT-I T cells that have undergone 1-4 divisions, scaled according to generation.*

g) *Cell counts over time for OT-I T cells that have undergone 5-7 divisions, scaled according to generation.*

h) *Cell counts over time for OT-I T cells that have undergone 5-8+ divisions, scaled according to generation.*

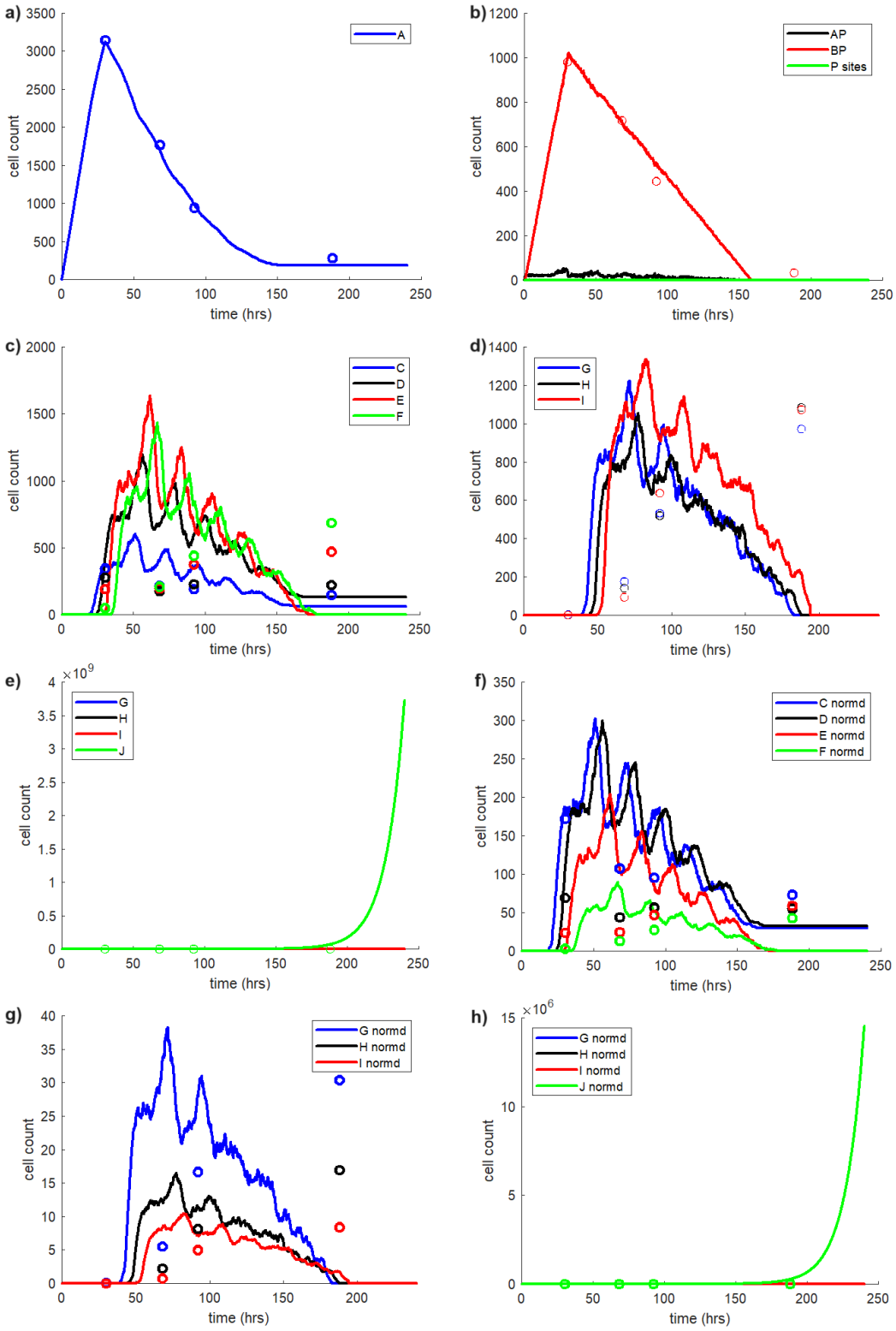

Figure 7: STORE.1 KO cell counts by generation.

a) Cell counts over time for naïve OT-I T cells.

b) *Cell counts over time for unbound APCs, APCs bound to Nur77^{GFP-} OT-I T-cells (AP), and APCs bound to Nur77^{GFP+} OT-I T cells (BP).*

c) *Cell counts over time for OT-I T cells that have undergone 1-4 divisions.*

d) *Cell counts over time for OT-I T cells that have undergone 5-7 divisions.*

e) *Cell counts over time for OT-I T cells that have undergone 5-8+ divisions.*

f) *Cell counts over time for OT-I T cells that have undergone 1-4 divisions, scaled according to generation.*

g) *Cell counts over time for OT-I T cells that have undergone 5-7 divisions, scaled according to generation.*

h) *Cell counts over time for OT-I T cells that have undergone 5-8+ divisions, scaled according to generation.*

In the STORE.1 model, both WT and KO cells had equal cohort numbers, for example, there are 6 cohorts in *G* cell counts in WT and KO cells, both around 50, 70, 90, 115, 135, 155 hours (Fig 5d, 7d). In STORE.2, the number of cohorts in a generation's cell count differs depending on the mouse host, such as WT *G* cells having 7 peaks, while KO *G* cells have only 4 peaks (Fig 4d, 6d). This difference, along with the other model-varying cohort dynamics are due to *BP* transitions, and the dynamics of P cells.

3.3. Variation in AP, BP, and P Dynamics Across STORE.1 and STORE.2

The *BP* cells transitions that generate two new *C* cells occur in pulses, producing the cohorts of daughter cells. These cohorts divide over similar timescales, and so the pattern of oscillations in one generation are carried over to the next.

As seen with in vivo data, the STORE.2 WT simulation had higher cell counts than KO simulations for all generations except *A*. The greater baseline metabolic activation (represented by a higher *cMYCMetabolicPower*) in WT cells lowered the number of c-MYC proteins required to advance a single cell through the pre-mitotic phases of the cell cycle. The resultant faster cell cycle progression enabled WT *BP* cells to more quickly divide to form *C* cells and recycle their *P* to the system. Faster WT *P* turnover meant that more *APs* were created that could go on to divide and drive-up overall cell counts, while simultaneously consuming the *A* cell population. Furthermore, STORE.1 WT simulations have more cohorts than KO simulations because the faster *P* turnover produces *APs* at a higher rate.

For KO simulations, the slower *P* turnover means that cells remain longer in the *BP* and *A* generations, and as a result, are more likely to leave the system via their respective leaving probabilities, further lowering overall cell counts.

These phenomena can be seen in the differing *BP* and *A* cell counts for WT and KO mice (Fig 8).

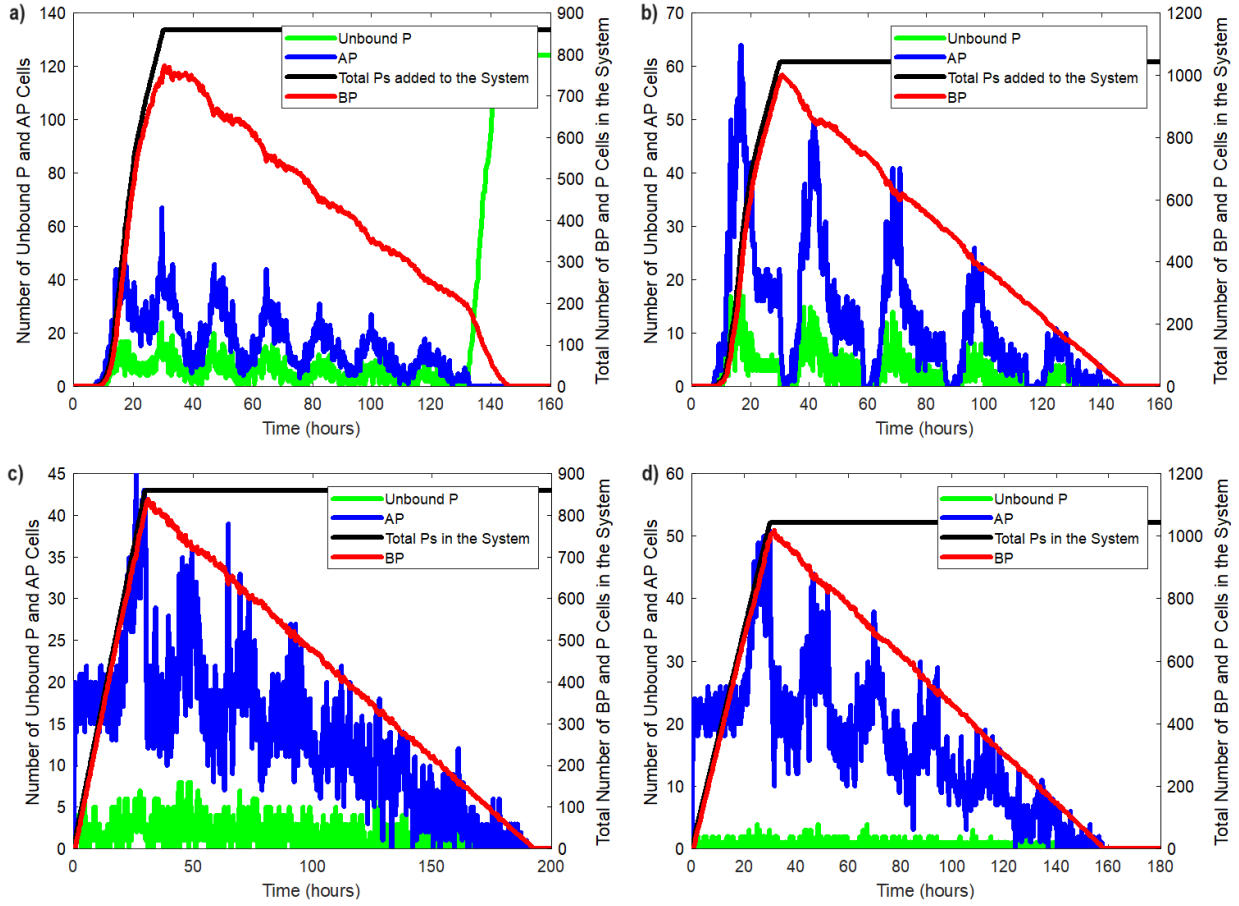

Figure 8: Overall counts for different states of P-cells

a) STORE.2 WT simulation of P-counts over time

b) STORE.2 KO simulation of P-counts over time

c) STORE.1 WT simulation of P-counts over time

d) STORE.1 KO simulation of P-counts over time

BP counts decline faster in STORE.2 KO cells at an almost linear rate towards zero, whereas STORE.2 WT *BP* decline is marked with several humps until 120 hours, whereby the cell count decline accelerates. At 120 hours, all STORE.2 WT *A* cells have left the system, precluding any further *A-P* binding, which not only causes *P* counts to rise, but halts the production of *BPs*, which had, until this point, counteracted both the leaving rate and transition rate (Fig. 8a). STORE.2

KO *BP* counts accumulate higher and decline faster than their WT counterparts due to a combination of longer cell cycle durations, and the *BP* leaving rate.

Decline for STORE.2 WT and KO *BPs* is not linear, as the count pulses in a regular, almost stepwise fashion, at a greater magnitude than the random fluctuations in the line. These pulses are coincident with the cohort peaks in *AP* and *P* counts, and number the same as the cohort peaks in *C* through *I* cell counts. Similarly, the STORE.1 *AP* and *P* counts fluctuate with the same cohort peaks as the WT and KO *C* through *I* cell counts. For both models, the shape of the cell count curves are set by the dynamics of *P* turnover.

3.4. Regression

Visual similarity aside, when a linear regression analysis is conducted on the in vivo cell counts and simulated cell counts for both STORE.1 and STORE.2, STORE.2 has an equivalent or higher R^2 value for all cell groups aside from KO *C-H* cell counts. R^2 values were calculated for each generational cluster: As, BPs, C-H, I, and F. Each is tightly correlated with the other cells in the group. To account for the effective doubling of cell counts for each generation, cell counts were normalized by the corresponding power of 2. As part of this, the *I-J* group was divided as *J* cells grow from all divisions 8+, and so would exert outsized influence on any regression for an *I-J* group.

Table 9: Regression values for different STORE models, stratified by cell generation.

Regression for As	
WT STORE.1 $R^2 = 0.875$	WT STORE.2 $R^2 = 0.8705$

KO STORE.1 $R^2 = 0.9684$	KO STORE.2 $R^2 = 0.9870$
Regression for BPs	
WT STORE.1 $R^2 = 0.9513$	WT STORE.2 $R^2 = 0.9318$
KO STORE.1 $R^2 = 0.9895$	KO STORE.2 $R^2 = 0.9892$
Regression for Cs-Hs	
WT STORE.1 $R^2 = 0.5988$	WT STORE.2 $R^2 = 0.7498$
KO STORE.1 $R^2 = 0.1571$	KO STORE.2 $R^2 = 0.03318$
Regression for Is	
WT STORE.1 $R^2 = 0.5847$	WT STORE.2 $R^2 = 0.5224$
KO STORE.1 $R^2 = 0.005323$	KO STORE.2 $R^2 = 0.6855$
Regression for Js	

WT STORE.1 $R^2 = 0.2466$	WT STORE.2 $R^2 = 0.3922$
KO STORE.1 $R^2 = 0.9998$	KO STORE.2 $R^2 = 0.9997$

While the STORE.2 model overall has equivalent or higher R^2 values than the STORE.1 model, it has a lower R^2 value when it comes to KO *C-H* cell counts. The STORE.1 KO simulations for generations *C-H* explain little variation among in vivo cell counts. The STORE.2 model KO dynamics share the overall shape as STORE.1 KO cells, but in addition, *C* to *H* cells appear several hours after in vivo data notes their appearance, and cells transition or leave the system several hours before in vivo data notes their disappearance. As a result, the cell count at these time points are zero, which further drive down the R^2 values.

R^2 values can normally indicate model fitting, but given the stochastic nature of both STORE models, and large variability in the test in vivo mouse cell count dataset, it is not an infallible metric by which to measure the applicability of the STORE models. As can be seen in following figures, both STORE.1 and STORE.2 cell counts vary depending upon the simulation, but not by the extent that the in vivo data varies. Whether the in vivo cell count variation reflects limitations to the experimental methods or true variation has yet to be determined.

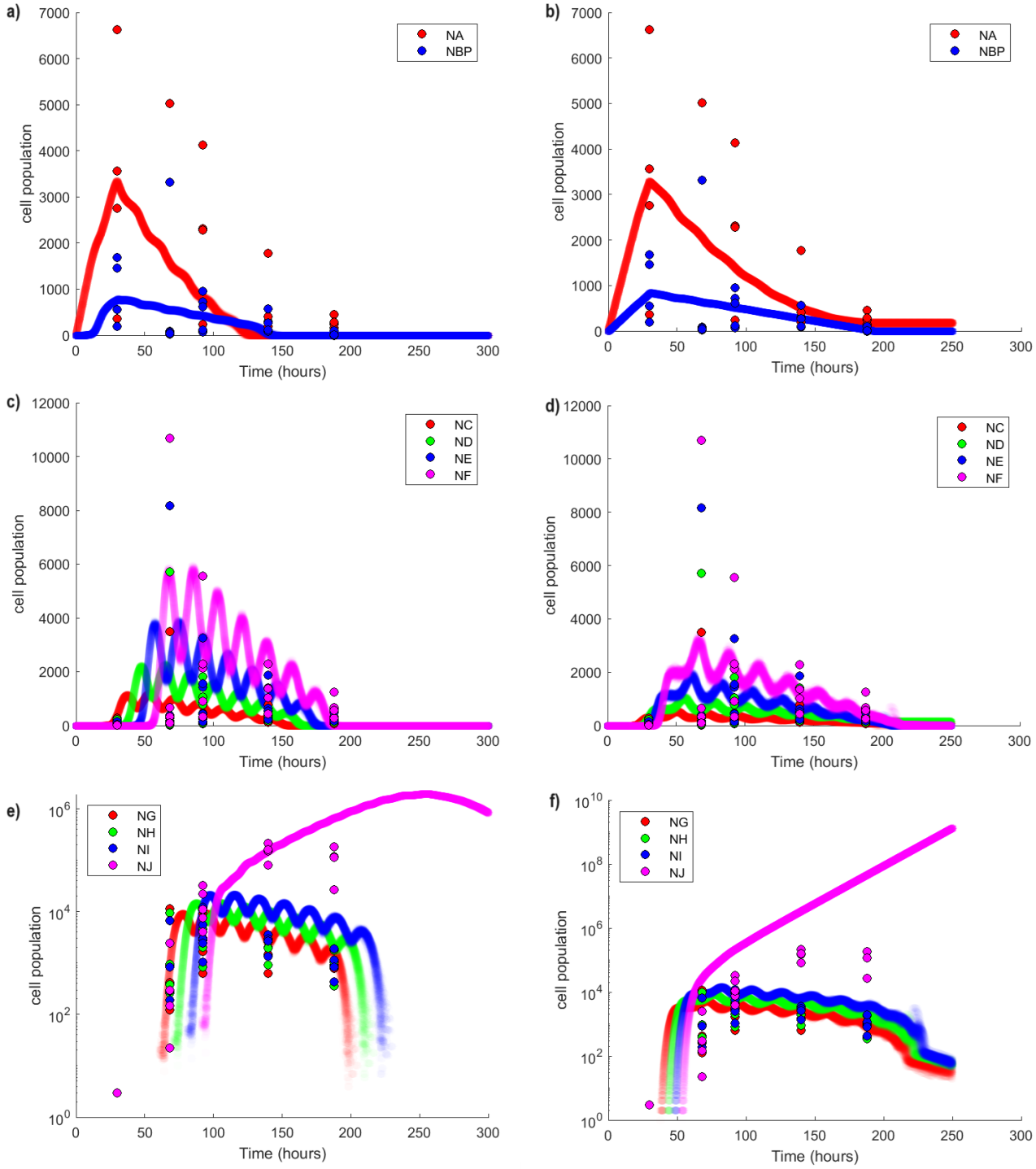

Figure 9: 50 simulations for the STORE.1 and STORE.2 models plotted against in vivo mouse data.

a) STORE.2 simulated cell counts over time for naïve OT-I T cells and APCs bound to Nur77^{GFP+} OT-I T cells (BP).

b) STORE.1 simulated cell counts over time for naïve OT-I T cells and APCs bound to Nur77^{GFP+} OT-I T cells (BP).

c) STORE.2 simulated cell counts over time for divisions 1-4 of OT-I T cells.

d) STORE.1 simulated cell counts over time for divisions 1-4 of OT-I T cells.

d) STORE.2 simulated cell counts over time for divisions 5-8 of OT-I T cells.

e) STORE.1 simulated cell counts over time for divisions 5-8 of OT-I T cells.

3.5. Cell Leaving

While the initial STORE.2 WT *D* cohort is twice the size of the initial *C* cohort, 2000 to 1000 cells respectively, the *E* cohort is only 3800 cells large, and the *F* cohort is only 6000 cells large. Even though each generation should be duplicate the last due to mitosis, the normalized cell counts for *E* to *I* cells are noticeably less than prior generations. The drop in expected cell count values is due to cell leaving rates that convert *E* to *J* generations to *K* cells. This dynamic is shared for *E* to *I* cells in STORE.1 WT simulations.

STORE.2 WT cells reach triple the overall cell population of KO cells. However, the magnitude of difference between WT and KO cell generations varies. Each WT cell generation reaches higher cell values than the previous, but KO cell counts drop from *E* to *H*. Though STORE.2 KO *C* and *D* cells have higher cell counts than their WT counterparts, *E* to *J* counts can be lower by an order of magnitude. While the elongated cell cycle means that *C* and *D* generation KO cells accumulate, surpassing their WT counterparts, the leaving rate for *E* through *H* cells is an order of magnitude greater in KO cells, quickly removing cells from these generations.

The rate of STORE.2 WT cell division is fast enough to produce effective doubling for *C* to *E* cell counts. In KO cells, only the *D* peak is double the size of the *C* peak. Leaving rates in the *E* peak, along with slower cell division, produce a peak only 1.07-fold higher than the *D* peak; the cells cannot divide faster than they leave, a phenomenon that continues to exert its influence to

ensure that each subsequent peak is lower than the last. Only the *I* peak is higher than the previous peak, due to *I-J* cells having a substantially lower leaving rate.

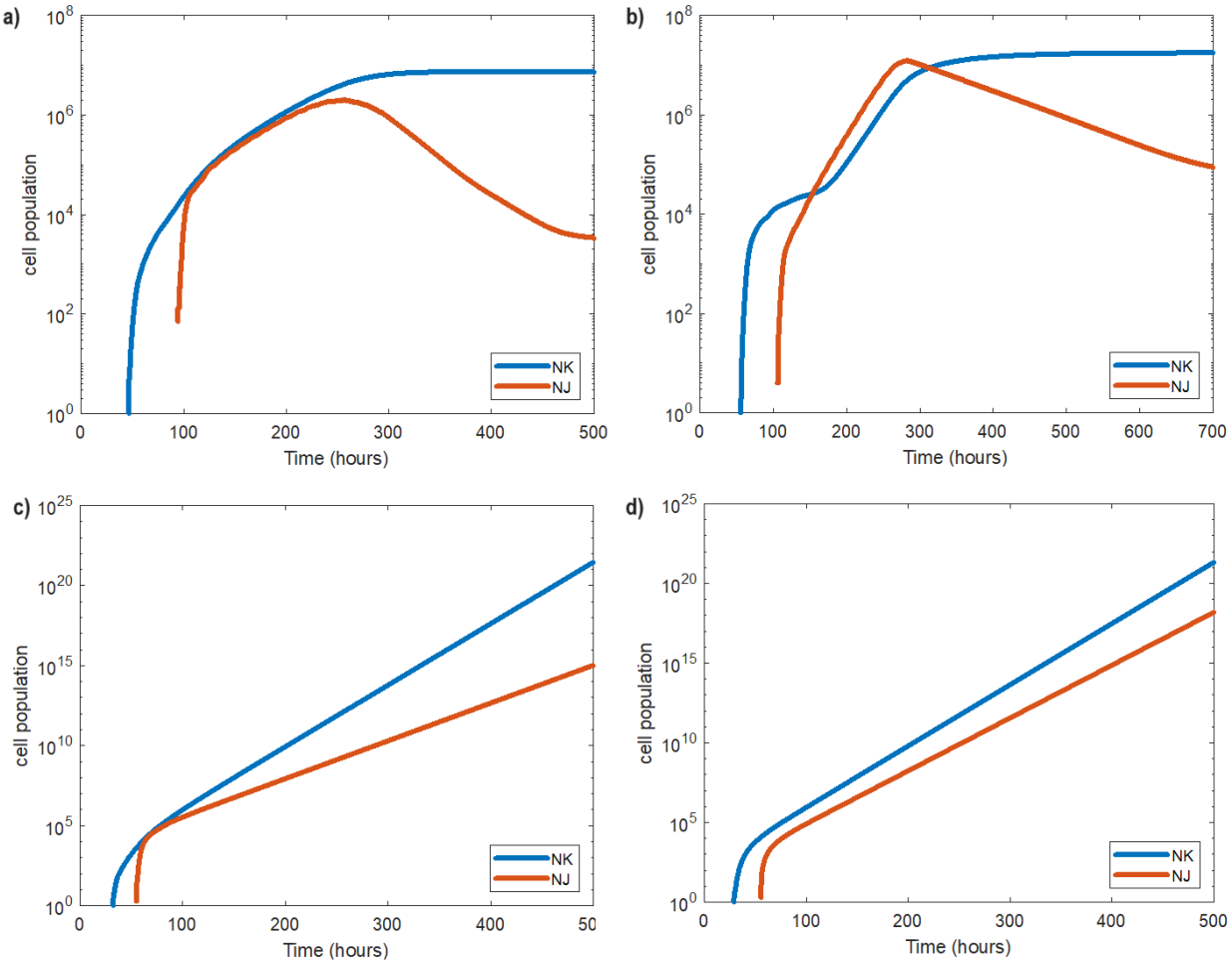

Figure 10: J and K cell counts versus time.

a) a STORE.2 simulation of WT J and K counts

b) a STORE.2 simulation of KO J and K counts

c) a STORE.1 simulation of WT J and K counts

d) a STORE.1 simulation of KO J and K counts

The runaway division in the STORE.1 model means that even though *I-J* leaving probabilities are equivalent for both STORE models, the resultantly enormous counts of *I-J* cells contribute tens of thousands of new *K* cells every timestep (Fig. 11).

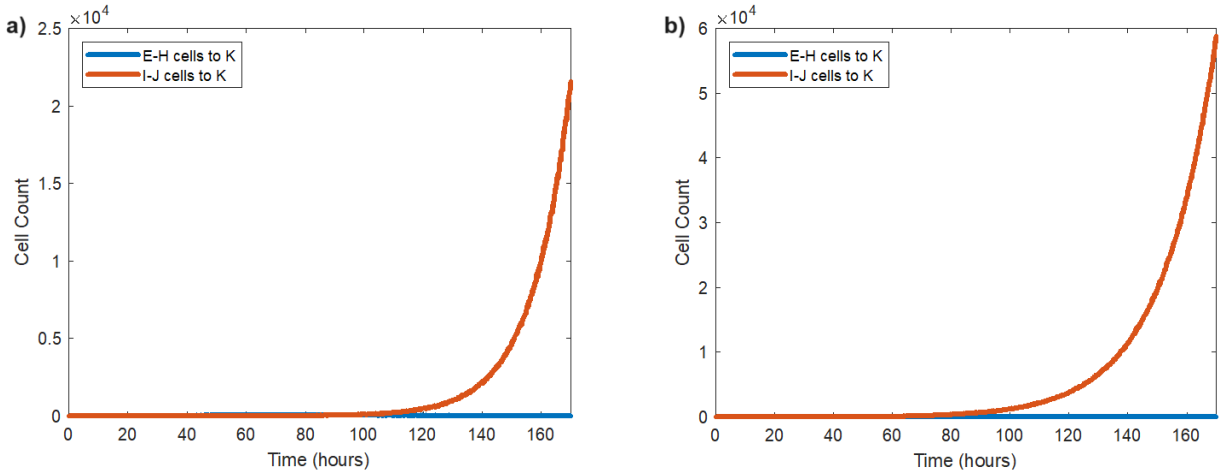

Figure 11: The number of E-H and I-J cells that transition to K per timestep in STORE.1 simulations.

a) WT simulation

b) KO simulation

By comparison, the acid-regulated cell division of the STORE.2 model means that *I-J* counts are lower, and the difference between *E-H* born *K* cells, and *I-J* born *K* cells, are only, or less than, an order of magnitude for WT and KO cells, respectively (Fig. 12).

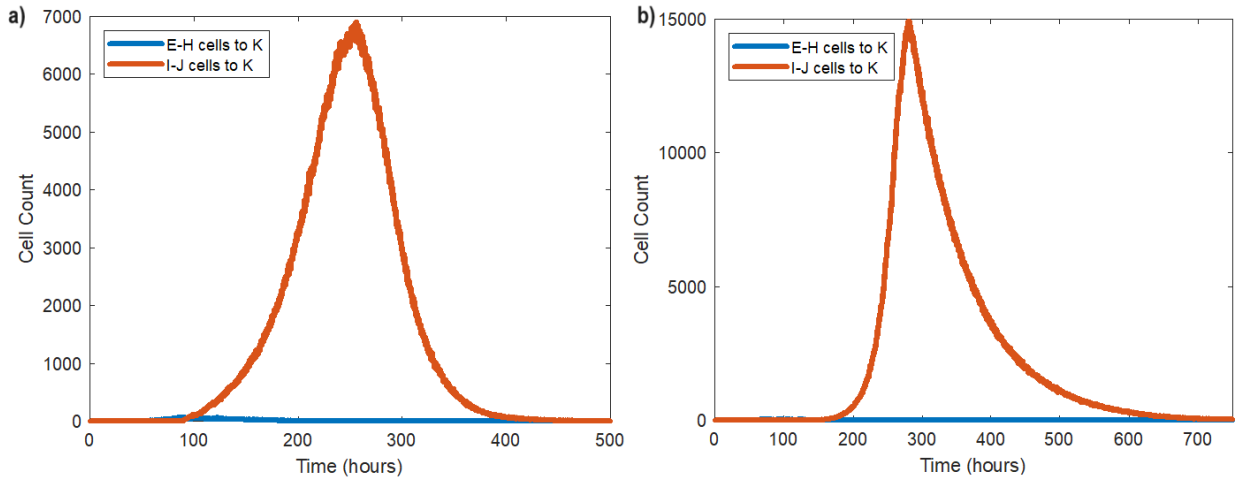

Figure 12: The number of E-H and I-J cells that transition to K per timestep in STORE.2 simulations.

a) WT simulation

b) KO simulation

The decline in I-J transitions to K for both WT and KO cells coincide with division cessation. It also correlates with the plateau and decline of J cell counts (Fig. 9, 10). In WT-residing cells, this division cessation occurs around 260-270 hours, while in KO-residing cells, division cessation stops around 280-290 hours. The exact cause of division cessation is the loss of c-MYC (Chapter 4).

3.6. References

1) Heinzel, Susanne, Tran Binh Giang, Andrey Kan, Julia M. Marchingo, Bryan K. Lye, Lynn M. Corcoran, and Philip D. Hodgkin. “A Myc-Dependent Division Timer Complements a Cell-Death Timer to Regulate T Cell and B Cell Responses.” *Nature Immunology* 18, no. 1 (January 1, 2017): 96–103. https://doi.org/10.1038/ni.3598.

Chapter 4: c-MYC Counts

Unlike the STORE.1 model, the STORE.2 model is capable of simulating and tracking characteristics of individual cells, including c-MYC. This chapter examines the dynamics of c-MYC production and decay in the STORE.2 model, as well as its impact on the extracellular environment.

4.1. Average c-MYC Counts for WT and KO Mice

There is scant literature reporting absolute c-MYC protein numbers in $CD8^+$ T-cells. There are results that show dividing WT T-cells express between 4000-8000 c-MYC molecules per cell 24 hours after stimulation.[1] WT c-MYC values 24 hours post activation in the STORE.2 model have c-MYC counts of approximately 7000-8000 proteins (Fig 4a). There aren't any c-MYC counts in literature or from in vivo experiments on KO c-MYC values, but the STORE.2 model simulates average KO c-MYC values that are approximately four times those found in WT c-MYC (Fig 13).

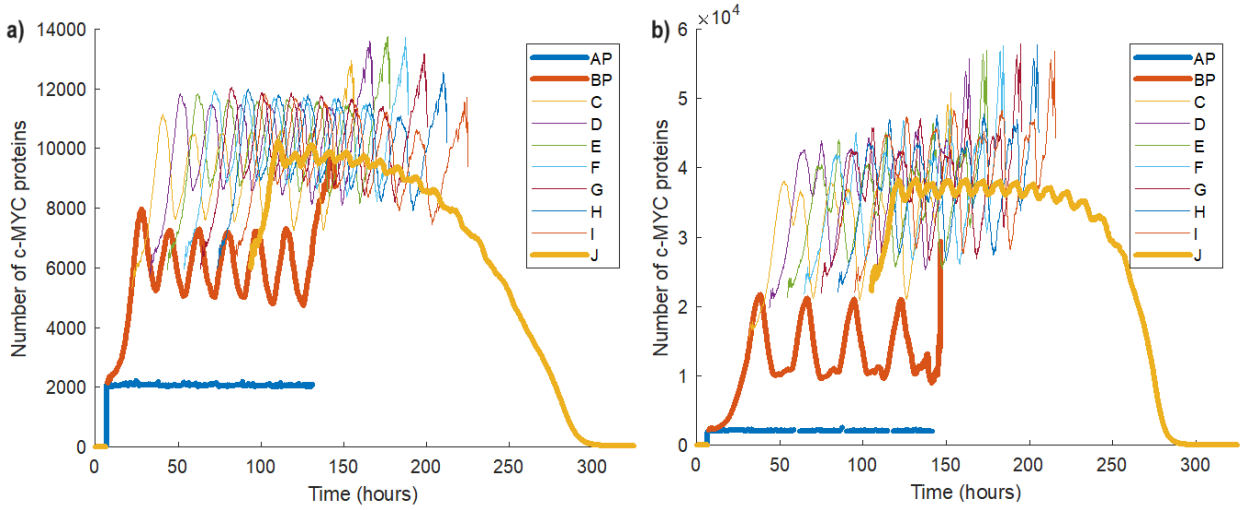

Figure 13: Overall c-MYC counts for all generations over time in the STORE.2 model.

a) WT simulation

b) KO simulation

Higher c-MYC values have been seen for OT-I T-cells transferred into IRF8^{--} mice, a condition that is reminiscent of the BATF3^{--} KO mice used in this study [unpublished data].

c-MYC counts grow during pre-mitotic phases of the cell cycle. In order to divide cells need to accumulate the store of duplicated organelles and metabolites, mathematically, this is defined as the area under the personal c-MYC count curve multiplied by the scalar multiplier *MI*. Simulated cells with low starting c-MYC at the start of G1 have longer pre-mitotic phases where c-MYC counts steadily grow, while cells with higher starting c-MYC at G1 are able to spend less time in the pre-mitotic phase.

c-MYC counts increase from the *AP* baseline until they plateau. WT cell c-MYC values plateau around 10000 c-MYC proteins per cell, while KO c-MYC plateaus around 38000 c-MYC proteins per cell. This plateau reflects the balance between the cells ability to import amino acids for c-MYC manufacture (AA_{Influx}), and the rate that metabolic pathways can be marshalled by c-MYC proteins (*MP*). At low acid-induced feedback impairment and high c-MYC, the unrestricted rapid influx of amino acid feeds into the high c-MYC. The c-MYC reaches such a high count that even when it is halved by mitosis, and decayed via the unopposed half-life, it has decreased back to the level that it started the previous generation with. If acid was instantaneously pulled from the system and never allowed to impact the rate of amino acid influx, cells would go on repeating the same c-MYC growth and decay cycles in perpetuity.

However, as the cell population within the system grows exponentially, so does the acid produced per timestep, lowering the pH of the microenvironment.

4.2. Acid Production

Acid production per timestep closely follows the total cell population until a critical point. When the cell population grows large enough that acid production impairs c-MYC feedback, fewer new c-MYC proteins are created to oppose the loss of proteins that result from c-MYC half-life. c-MYC values plummet, and thus the glycolytic rate plummets, impairing the production of lactic acid, and thus decoupling acid production per timestep from the overall cell population (fig 14).

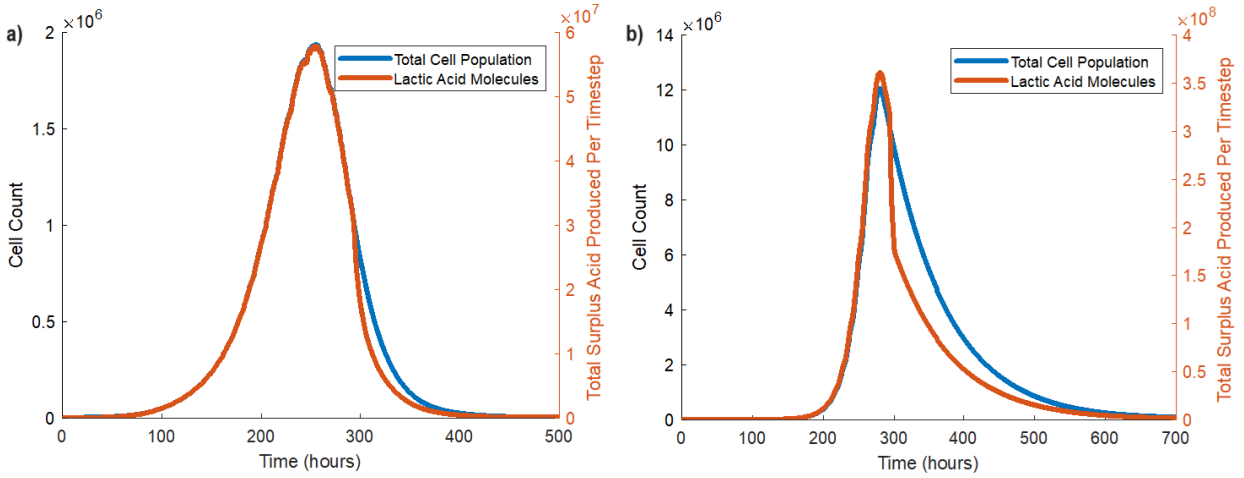

Figure 14: Acid production and system-resident cell population over time.

a) WT simulation

b) KO simulation

Both the average c-MYC count and acid production per timestep for KO cells decline faster than for cells in WT mice. STORE.2 KO cell counts are more resilient to acid-induced c-MYC inhibition due to the higher c-MYC counts. When acidification begins to diminish c-MYC feedback, the higher c-MYC counts can still produce significant additional c-MYC that counters the half life. Cells continue to divide and further drive-up lactic acid production until peak KO acid per timestep is seven-fold greater than WT peak acid per timestep. This suggests that KO mice would have more acidic sites of OT-I T-cell proliferation.

Despite initial KO c-MYC count resilience against acid-induced feedback inhibition, eventually the concentration of lactic acid gets too high, and feedback begins to be markedly impaired. Due to lower leaving rates for KO *J* cells, acid-producing cells remain in the system longer than their WT counterparts, ensuring that when KO c-MYC counts decline, it is more rapid than the c-MYC decline in WT cells. However, there can come a point where enough cells have left that the inhibition lessens, as seen in how KO cell lactic acid begins to slow its descent (Fig. 14b). At that point, cell counts and the cumulative lactic acid begin to recouple, though the impairment is still substantial enough that c-MYC cannot exponentially grow via positive feedback, and eventually all cells remain pre-mitotic, capable only of leaving the system. This marks the end of the proliferative phase.

There are two phenomena that occur with c-MYC averages at late, acid-impaired, time points. 1) The *C-I* c-MYC averages begin to rise as the metabolic power of a single c-MYC protein plummets, and division requires ever increasing c-MYC counts. 2) *J* c-MYC averages steadily decline. While individual *J* cells are increasing their c-MYC counts, they are not doing so in phase, and so the sheer number of cells prevent erratic fluctuations of the average, unlike the small number of remaining late-stage *C - I* cells that exert outsized influence on the c-MYC average.

This can be seen when c-MYC averages are plotted against c-MYC counts for all members of a cell generation (Fig. 15). Individual cell c-MYC counts for *J* cells at any specific point are equivalent with c-MYC counts for contemporaneous cell generations.

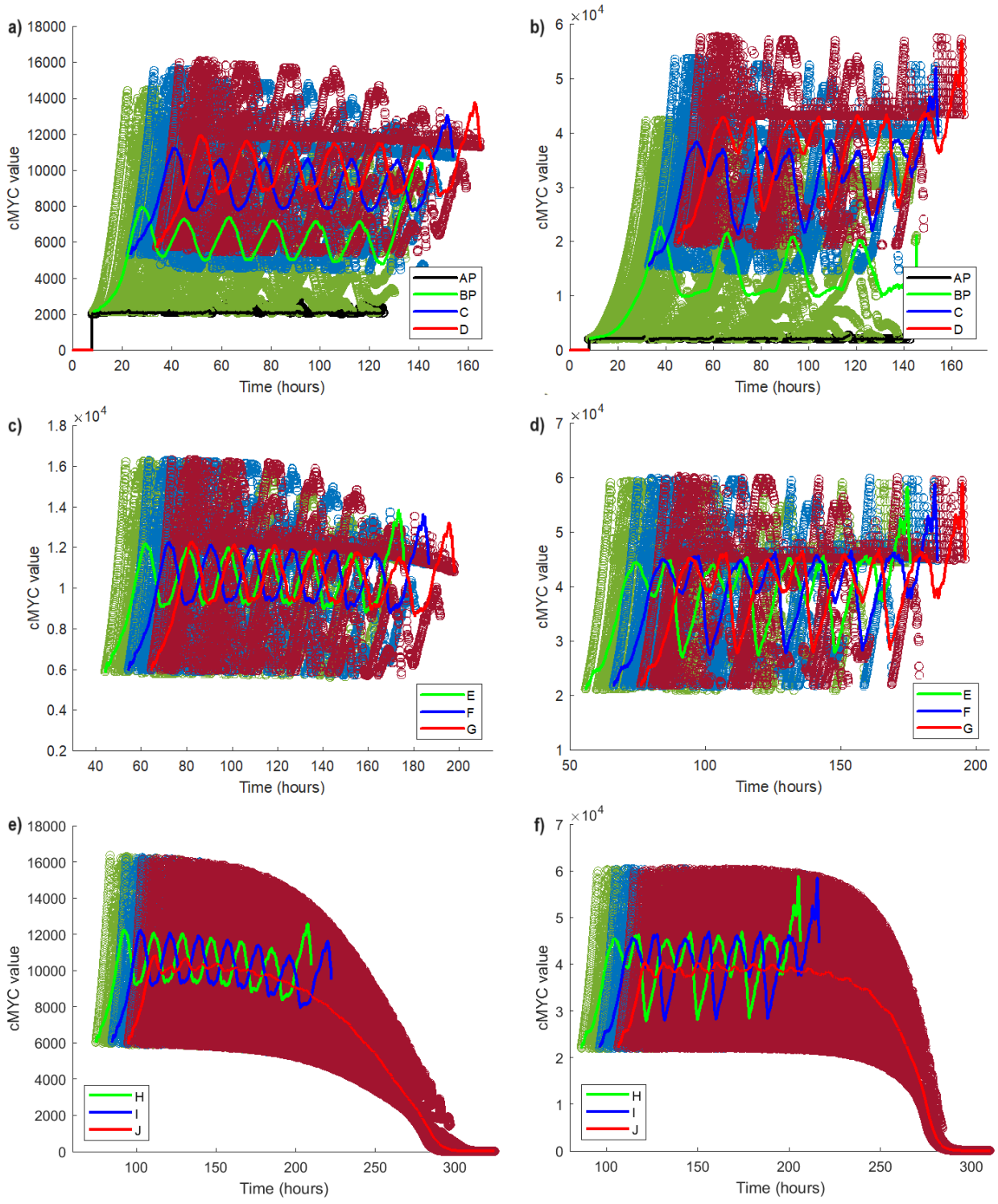

Figure 15: Average c-MYC counts plotted against c-MYC values for all individual cells of a given generation.

a) WT simulated c-MYC over time for APCs bound to Nur77^{GFP-} OT-I T-cells (AP), APCs bound to Nur77^{GFP+} OT-I T-cells (BP), and OT-I T-cells that have undergone 1-2 divisions.

b) KO simulated c-MYC over time for APCs bound to Nur77^{GFP-} OT-I T-cells (AP), APCs bound to Nur77^{GFP+} OT-I T-cells (BP), and OT-I T-cells that have undergone 1-2 divisions.

c) WT simulated c-MYC counts over time for cells that have undergone 3-5 divisions.

d) KO simulated c-MYC counts over time for cells that have undergone 3-5 divisions.

e) WT simulated c-MYC counts over time for cells that have undergone 6-8+ divisions.

f) KO simulated c-MYC counts over time for cells that have undergone 6-8+ divisions.

Individual c-MYC counts for KO cells vary more than c-MYC counts for WT cells. Since KO cells require a higher quantity of c-MYC in order to divide, a greater amount of c-MYC is removed due to the half-life and halving between daughters during mitosis.

Just as WT cells report more cell count fluctuations, there are more oscillations in WT c-MYC counts over time than KO cells. Average c-MYC counts fluctuate, with the same number of peaks as the cell count for their corresponding generation. Likewise, the peaks from one generation to the next are staggered in time. Cells of one cohort grow their individual c-MYC counts over time until, at the height of their c-MYC count, they transition to the next generation. As high c-MYC count cells leave, the averages fall to the lower c-MYC counts that belong to the next cohort of cells that have transitioned into that specific generation. The fluctuations in average c-MYC counts do not represent changes to system-wide c-MYC accumulation and decay dynamics, rather they reflect the clustering of cells into cohorts. At earlier generations, these cohorts are more easily discerned (Fig 13), but with *J* cells it is nearly impossible to discern any cohort structure. This is not because no such structure exists, but because the *J* generation contains all the different 8+ divisions, with their respective cohorts overlapping, obscuring any greater structure, and limiting the magnitude of fluctuations. Indeed, at earlier time points the *J* c-MYC average fluctuates in line with previous generations but is quickly smoothed out by the growing cell population.

4.3. References

1) Marchingo, Julia M, Linda V Sinclair, Andrew JM Howden, and Doreen A Cantrell. "Quantitative Analysis of How Myc Controls T Cell Proteomes and Metabolic Pathways during T Cell Activation." Edited by Ellen A Robey, Tadatsugu Taniguchi, Ellen A Robey, and Jeroen P Roose. *ELife* 9 (February 5, 2020): e53725. https://doi.org/10.7554/eLife.53725.

Chapter 5: Cell Division Dynamics

5.1. Background

CD8+ T-cells are generally considered to divide 7-10 times at minimum.[1] The maximum number of divisions for some T-cells has been estimated to be 137 divisions, though the circumstances behind the resulting enormous cell population are artificial and highly selective.[2]

During DNA replication, DNA polymerase cannot replicate the end of the DNA strand.[3] To protect against gene loss, at the end of linear chromosomes are repetitive nucleotide sequences called telomeres.[3] With each division telomeres are shortened until a critical length, whereby senescence or apoptosis occur through DNA damage pathways.[3] The number of divisions until telomeres are too short is termed the Hayflick Limit, which was first determined in fibroblasts to be 40-60 divisions, and can vary for different cell types and species.[4] Notably, memory T-cells may not be subject to a Hayflick limit; Soerens et al. cultured vesicular stomatitis virus N52-59-specific CD8+ T-cells in CD45.1^{+} C57Bl/6 female mice for 60 days, allowing for clonal expansion and contraction, and then transferred some of the remaining memory cells into new infected mice.[2] This was repeated >50 times until the T-cell lineage had outlived the original mice.[2] Furthermore, cells were observed to have maintained telomere length without undergoing malignant transformation.[2] Whether this result is applicable to effector T-cells is yet to be determined, and requires further examination of the dynamics underpinning cell death (6.1.).

5.2. Cell Cycle Duration Dynamics

In the STORE.2 model it is possible to examine the length of time (in hours) that individual cells spend progressing throughout the cell cycle over different generations, and at different simulation times.

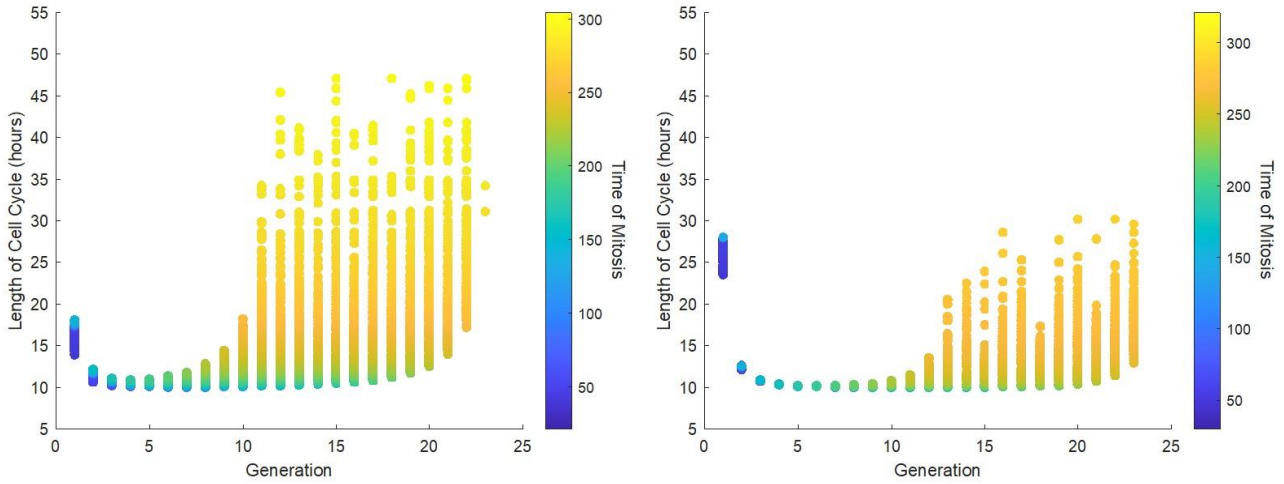

Figure 16: Cell cycle durations for different generations of cells

a) WT simulations

b) KO simulations

In early generations, on average, KO cells take longer to progress throughout the cell cycle than WT cells, but with successive generations, progress faster until reaching an average cell cycle duration of approximately 10 hours. WT cells progress faster than KO cells for several generations, until, on average, cell cycle duration begins to increase, outpacing KO cell cycle duration of the same generation. Early WT cell cycle rapidity is only regarding the average duration, as both WT and KO cells have a wide range of cell cycle durations in early generations.

As WT cells face increasing microenvironmental acidity, cell cycle durations gradually grow, with divisions post 250 hours lengthening beyond the long cell cycle durations of *AP-BP* cells. Indeed, c-MYC counts for *J* cells post 250 hours begin to drop first to the level of *BP* cells, and then even lower. Cells are able to complete a few divisions in the face of elevated acidification, but eventually, c-MYC levels decline to a point where the cell cannot advance all the way to the G2/M restriction point, and so exits its proliferative phase.

The comparative rapidity that c-MYC counts in KO cells decline due to elevated lactic acid production means that cells have less time to undergo several rounds of extended cell division like their WT peers. While WT *J* c-MYC averages begin to drop around 150 hours and reach 0 c-MYC proteins at 300 hours, KO *J* c-MYC averages begin to drop at 220 hours and reach 0 c-MYC proteins in 300 hours, giving KO cells 70 fewer hours to divide. Indeed, the acid-extended division durations of KO cells are substantially less than the durations of WT cells.

5.3. Minimum Cell Cycle Durations

Cell cycle durations reach a minimum duration of 10 hours when cells reach equilibrium with c-MYC (Fig 16). WT cells reach c-MYC equilibrium faster than KO cells, as KO cells take longer to reach their peak c-MYC levels. Judging by the division durations, KO cells only reach the peak c-MYC levels by generations *E* and *F*, while WT cells are at the peak levels by the *C* generation.

Just as the peak c-MYC level is set by the ratio of baseline amino acid influx and the metabolic power of a single c-MYC protein, so too is the minimum division duration (Fig 17). As a cell's baseline rate of amino acid influx increases, as it gets better at importing the materials to manufacture c-MYC, cells can complete division faster, and progress through more divisions before the half-life and acidification drains the cell's c-MYC count. If a cell imports too few amino acids, then it cannot manufacture enough c-MYC proteins to resist the half-life and quickly loses its c-MYC, whereas if a cell imports amino acids too quickly it speeds through the cell cycle and produces a large effector population that prematurely terminates the proliferative phase via acid production.

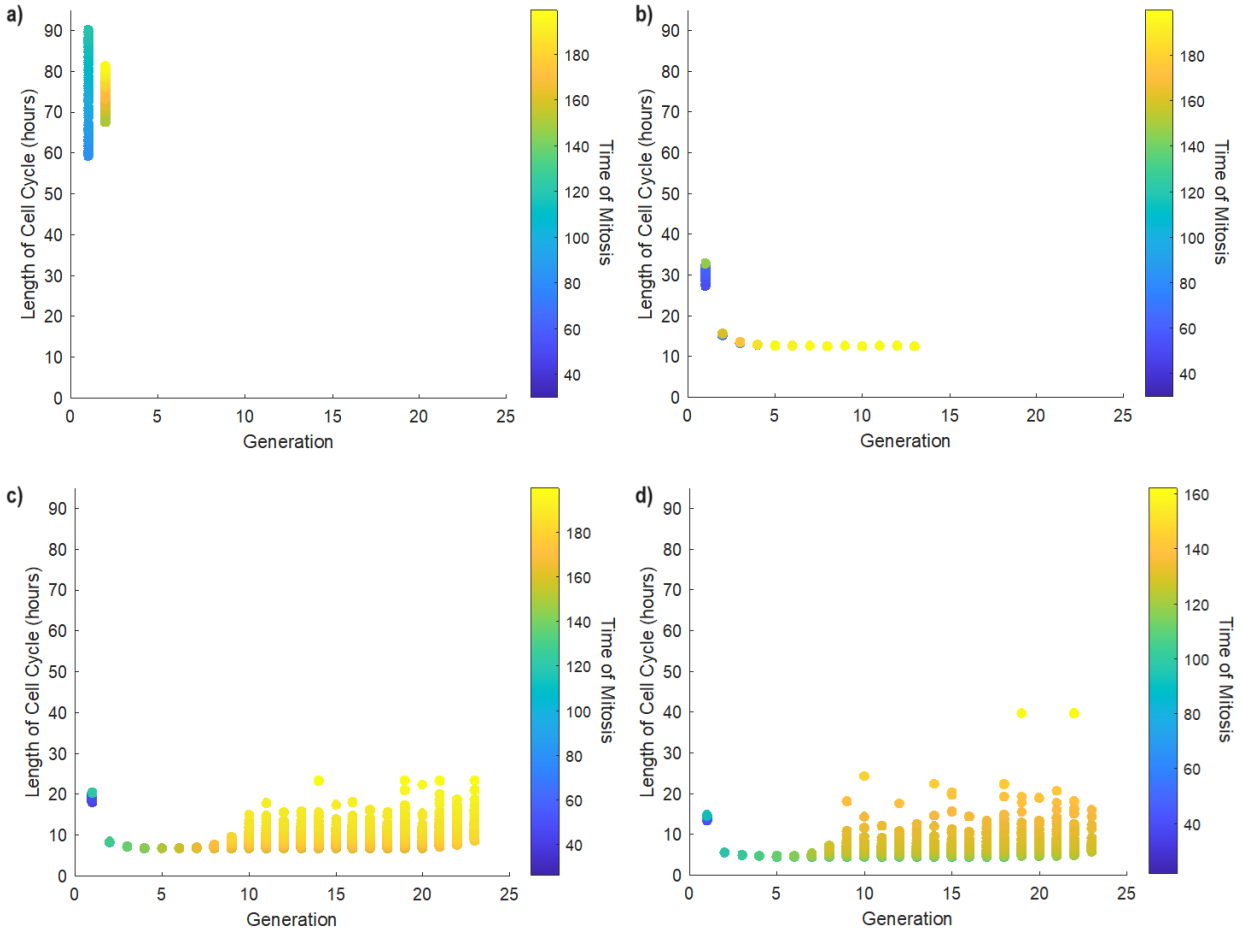

Figure 17: Minimum division duration is a function of the ratio of amino acid influx to metabolic "power."

a) *WT simulation where the ratio is: 1.158 X 10^8*

b) *WT simulation where the ratio is: 1.457 X 10^8*

c) *WT simulation where the ratio is: 1.855 X 10^8*

d) *WT simulation where the ratio is: 2.310 X 10^8*

5.4. Percentage of Mitotic Cells

As part of modelling the differing dynamics that govern c-MYC during G1-G2 and M phase, the STORE.2 model tracks whether individual cells are undergoing mitosis. For both WT and KO simulations, less than 25% of cells are undergoing mitosis at any one time.

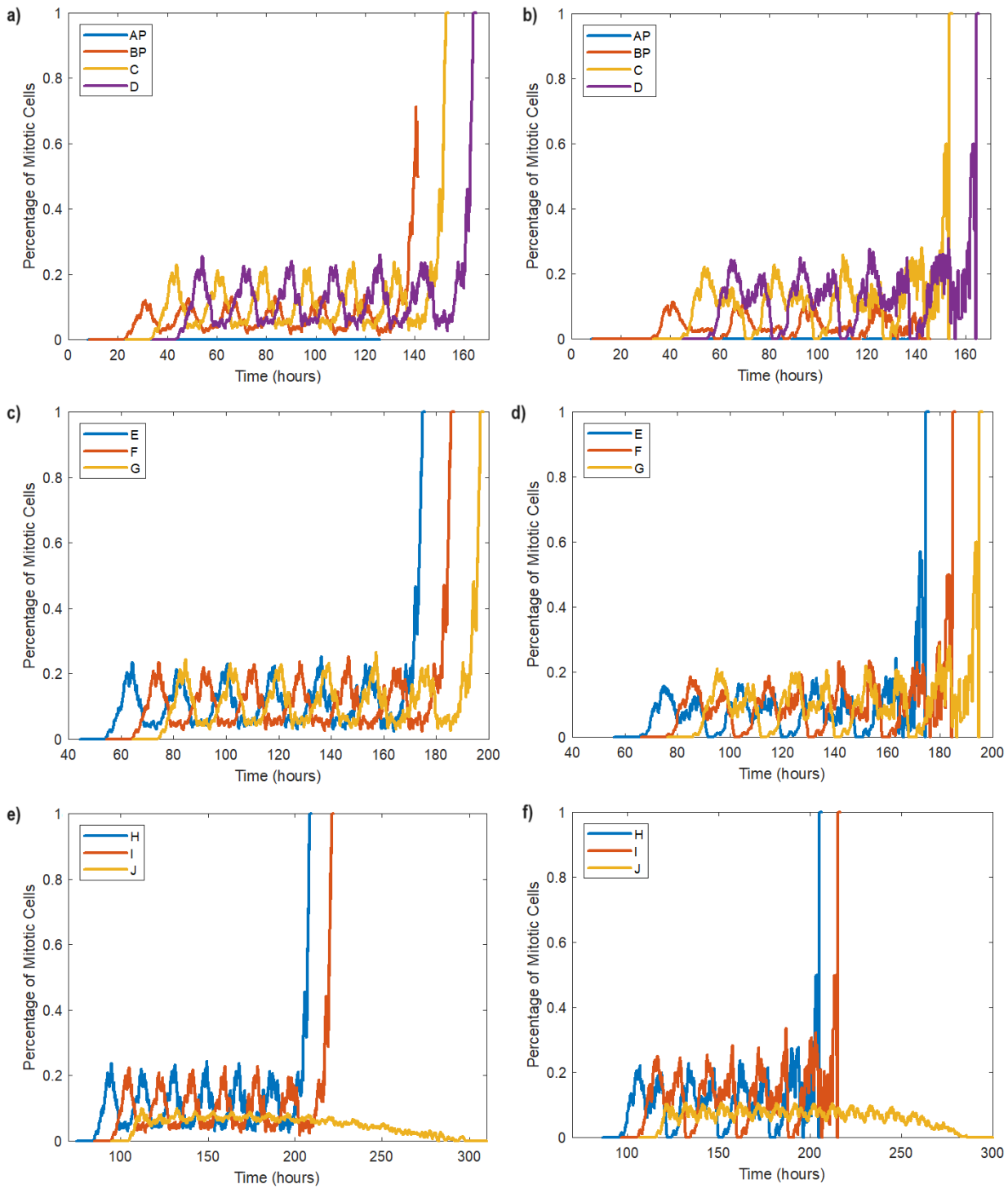

Figure 18: Percentage of mitotic cells per generation

a) WT simulated percentage mitotic cells over time for APCs bound to Nur77^{GFP-} OT-I T-cells (AP), APCs bound to Nur77^{GFP+} OT-I T-cells (BP), and OT-I T-cells that have undergone 1-2 divisions.

b) KO simulated percentage mitotic cells over time for APCs bound to Nur77^{GFP-} OT-I T-cells (AP), APCs bound to Nur77^{GFP+} OT-I T-cells (BP), and OT-I T-cells that have undergone 1-2 divisions.

c) WT simulated percentage mitotic cells over time for cells that have undergone 3-5 divisions.

d) KO simulated percentage mitotic cells over time for cells that have undergone 3-5 divisions.

e) WT simulated percentage mitotic cells over time for cells that have undergone 6-8+ divisions.

f) KO simulated percentage mitotic cells over time for cells that have undergone 6-8+ divisions.

WT and KO mitotic percentages fluctuate in line with fluctuations of cell counts. The peaks of mitotic percentage fluctuations occur at the same time as the troughs of the cell count fluctuations.

For both WT and KO cells, generation *C* through *I* reach 100% mitotic cells. This is because while some cells may leave the system prematurely, the very last cell of that generation reaches the G2/M checkpoint. By comparison, *BP* cell counts disappear via the leaving rate before they can transition, and thus do not reach 100% mitotic cells. *J* cells do not reach 100% as acid impairment prevents late-stage *J* cells from progressing through the cell cycle.

For WT cells, the fluctuations for each generation grow in amplitude; while 10% of *BP* cells are at most mitotic, 20% of *I* cells are mitotic. KO cell fluctuations similarly grow with generation, from approximately 10% of *BP* cells being mitotic at most, to 25% of *I* cells being mitotic at most. For both WT and KO cells, mitotic percentages for *J* cells fluctuate around 5%.

5.5. References

1) Kaech, Susan M., and Rafi Ahmed. “Memory CD8+ T Cell Differentiation: Initial Antigen Encounter Triggers a Developmental Program in Naïve Cells.” *Nature Immunology* 2, no. 5 (May 2001): 415–22. https://doi.org/10.1038/87720.

2) Soerens, Andrew G., Marco Künzli, Clare F. Quarnstrom, Milcah C. Scott, Lee Swanson, J. J. Locquiao, Hazem E. Ghoneim, et al. “Functional T Cells Are Capable of Supernumerary Cell Division and Longevity.” *Nature*, January 18, 2023. https://doi.org/10.1038/s41586-022-05626-9.
3) Rodriguez-Brenes, Ignacio A., Dominik Wodarz, and Natalia L. Komarova. “Quantifying Replicative Senescence as a Tumor Suppressor Pathway and a Target for Cancer Therapy.” *Scientific Reports* 5, no. 1 (December 9, 2015). https://doi.org/10.1038/srep17660.
4) Jin, Kunlin. “Modern Biological Theories of Aging.” *Aging and Disease* 1, no. 2 (August 1, 2010): 72–74. https://www.ncbi.nlm.nih.gov/pmc/articles/PMC2995895/.

Chapter 6: Next Steps

The STORE.2 model offers increased explanatory power, but by no means does it capture all of the nuances of c-MYC dynamics over the course of the cell cycle and proliferative phase. c-MYC is an essential regulator of cell division and metabolic reprogramming of $CD8^+$ T-cells, but it does not act alone in setting the length of the T-cell proliferative phase.

6.1. Regulators of Apoptosis

The Bcl-2 family represents a group of pro and anti-apoptotic proteins, including the eponymous anti-apoptotic Bcl-2 and pro-apoptotic BIM. Apoptotic BIM proteins induce effector pore-forming proteins called BAX/BAK to punch holes in, and thus depolarize the mitochondrial membrane to trigger cell death and are otherwise sequestered by anti-apoptotic proteins like Bcl-2.[1] This sequestration occurs via physical binding of BIM by Bcl-2 onto the mitochondrial membrane.[2]

Naïve T cells, specifically, were highly reliant on BCL-2 for survival, and sensitive to Bcl-2 inhibition. Memory CD8+ T-cells are also more reliant on Bcl-2 than memory CD4+ T-cells.[1]

Differing levels of BIM and Bcl-2 had little effect on the other's level of mRNA expression, but it did alter the amount of protein found in the cell, indicating BIM and Bcl-2 exert post-transcriptional control over one another. Excess Bcl-2 is inhibited by pathways dependent upon the level of BIM.

T-cell stimulation by antigen can lead to a doubling of Bcl-2, whereas there is no consequent rise in the amount of BIM, indicating that T-cell stimulation has a way of exerting independent control over Bcl-2 levels to ensure survival. This effect must drop off as just prior to cell death, Bcl-2 levels fall by ~50%.[2]

T-cells responding to an antigen can benefit from a secondary unrelated infection by the resultant rise in cytokine mRNA (IL-2, IL-7, IL-15, and IL-4). These individual cytokines may add together via Bcl-2 upregulation to promote survival.[3]

Bcl-2 stabilizes BIM via binding the normally unstructured protein, consequently preventing cell death by occupying its binding sites. BIM is elevated following T-cell stimulation, and so it is only cells with higher Bcl-2 that are capable of surviving. In these cells, when Bcl-2 is impaired slightly, cell death quickly proceeds.[4]

Of note, extremely elevated c-MYC levels can be apoptotic via BIM, but these levels are seen primarily in tumours, and are above the necessary levels of T-cell proliferation.[5]

6.2. Additional Rounds of Proliferation

Without death timers, the STORE.2 WT model can produce additional rounds of clonal expansion (every 1/5 simulations) through predator-prey dynamics. WT cells possess a ratio of amino acid influx to c-MYC metabolic power that enables cells to recover c-MYC levels from the lowest point following the acid-induced decay. c-MYC levels decline before cell counts decline. The reduced c-MYC levels are low enough that even the dropping cell counts remain high enough to produce acid-induced c-MYC feedback inhibition, in essence, the distance between the individual c-MYC curves and the cell count curves is large enough that the cell cannot grow its c-MYC. If a *J* cell had sufficiently high c-MYC when c-MYC counts overall began to plummet according to the 2.5-hour half-life, then there is a chance that the individual c-MYC decay curve will begin to close the gap and enable the cell's c-MYC to grow once more.

By comparison, the base amino acid influx of KO cells is too low to enable any recovery as c-MYC counts decay much faster (Fig 13b).

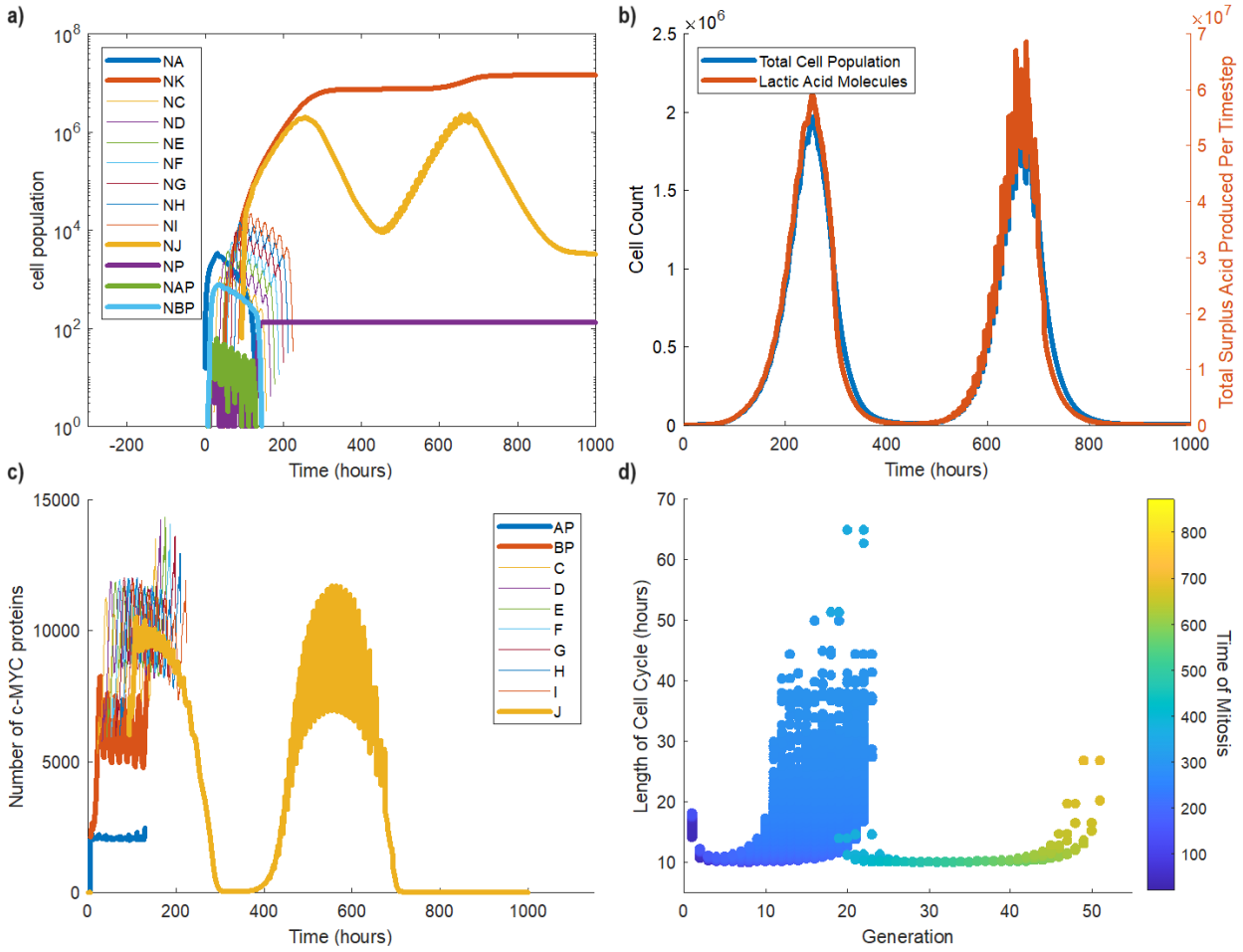

Figure 19: Dynamics associated with one additional round of cell division.

a) Cell counts for each generation.

b) Acid production and system-resident cell population over time.

c) Average c-MYC counts for each generation over time.

d) Division duration for each generation.

Occasionally only one additional expansion phase will occur. Of the thousands of *J* cells that remain, comparatively few cells have high enough c-MYC to enable the recovery (Fig. 20). These cells quickly expand into a clonal population of a similar size and scale as the first expansion phase. The second expansion phase reaches 50+ generations. Cell division occurs approximately 100 hours after the first expansion phase (Fig 19d).

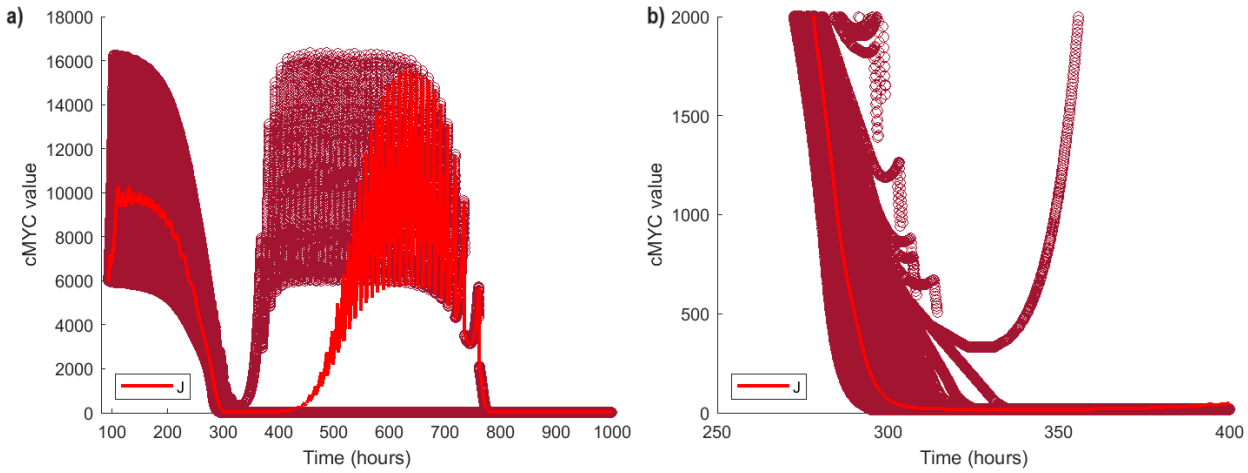

Figure 20: Average c-MYC values plotted against individual c-MYC values.

a) Average and individual c-MYC values plotted over all time.

b) Average and individual c-MYC values over the beginning of the second expansion phase.

WT cells can also undergo two rounds of cell expansion following the initial expansion phase. WT cells in the third expansion phase reach 59 generations, and once more, divide approximately 100 hours after the second round of cell division ends.

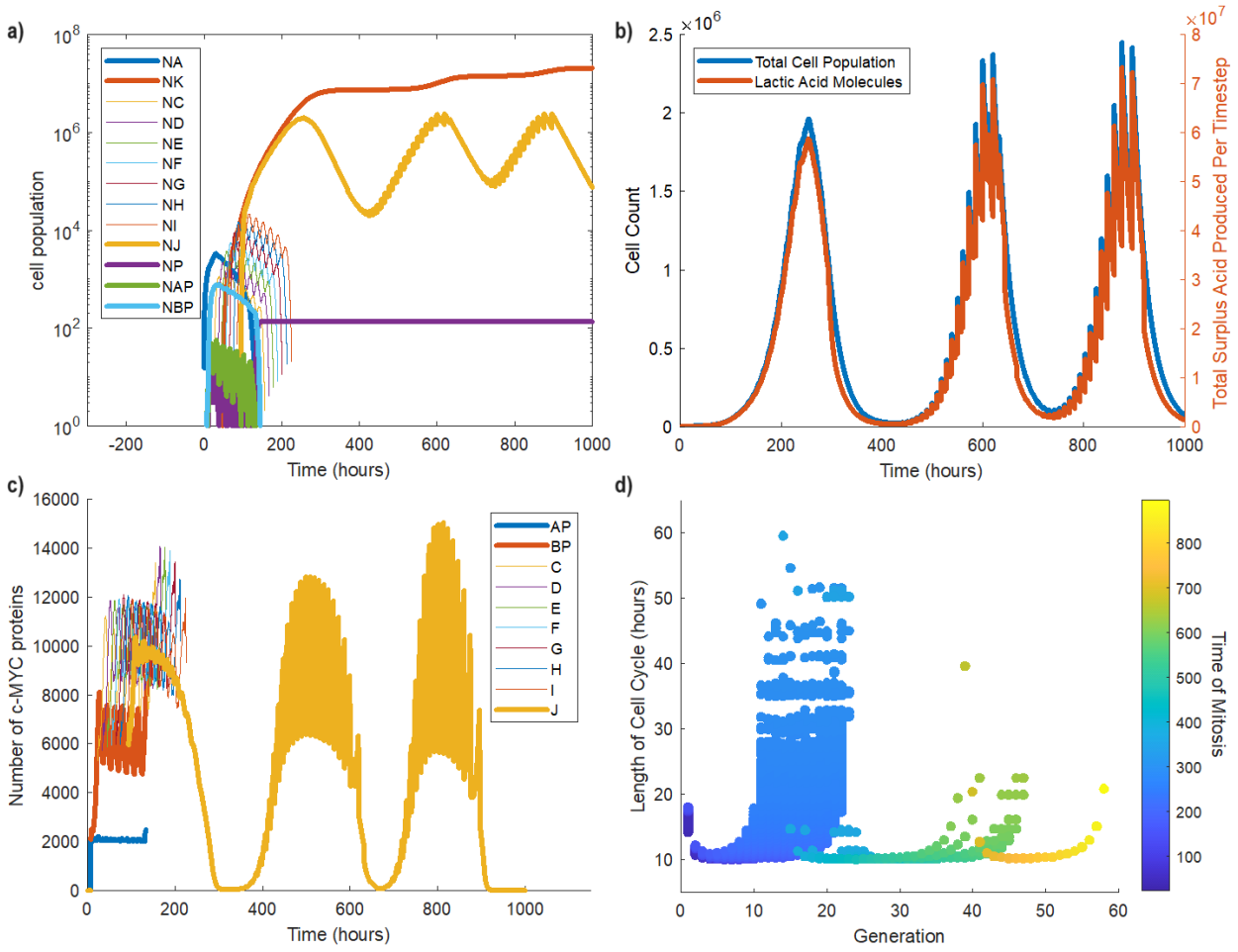

Figure 21: Dynamics associated with two additional rounds of cell division.

a) Cell counts for each generation.

b) Acid production and system-resident cell population over time.

c) Average c-MYC counts for each generation over time.

d) Division duration for each generation.

6.3. MAX

c-MYC is activated by dimerizing with MAX, enabling it to bind to DNA Enhancer-Boxes, attracting the Transformation/Transcription Domain-Associated protein that acetylates histones

(DNA tags that wrap up DNA into a tight bundle), opening up the strand for transcriptional machinery access.[6-8]

MAX can bind to other proteins such as the MAD family, Mnt, and Mga which compete with c-MYC for MAD binding sites with equal affinity.[7,9] However, there is evidence that during proliferation and differentiation, that only a small proportion of MAX is occupied by MAD proteins, despite MAD being detectably upregulated. Furthermore, mechanisms exist to sequester MAD proteins, pointing to several ways in which c-MYC inhibition is limited during proliferation.[8]

In the STORE.2 model, MAX is not modelled. Since the main c-MYC competitor for MAX binding sites is sequestered in proliferating cells, MAX is assumed to not be a limiting factor on c-MYC's ability to augment metabolic pathways. Since the model does not account for the limited inhibition that MAD-MAX binding produces for c-MYC activity, it is likely that the STORE.2 model overestimates the MP parameter.

6.4. Limitations

Currently, c-MYC parameters are deterministic, with each daughter cell being complete clones of each other. c-MYC parameters should have corresponding probability distributions that determine, for example, the efficacy of amino acid influx. This will provide increased stochasticity to the STORE.2 model and reflect the fact that daughter cells are not perfect mathematical clones of one another. Further in vivo experiments will need to be conducted in order to determine how c-MYC proteins are divided between daughter cells. Unequal c-MYC partitioning would introduce more heterogeneity into the cell population and bring the simulation closer in line with immunological reality.

Further work will need to introduce differentiation into the model, as T-cells specialize to create different effector subtypes, and memory cells. Additionally, while the STORE.2 model can

simulate division cessation, it cannot truly simulate the contraction phase. Measures of apoptosis will need to be introduced, chiefly Bcl-2, BIM, and Survivin.[10,11] CD8+ proliferation peaks around 7 days, whereupon T-cells begin to die during the contraction phase.[12]

To improve run-time for simulations, every single cell wasn't tracked. Instead, a maximum of 4377 "cells" for WT and 4458 "cells" for KO are modelled. This is the maximum number of *A* cells. Cells are assumed to be clonally identical, and so all daughter cells and descendants of a single *A* cell are grouped together. Rather than individually track 8 variables for 10^6 cells, the STORE.2 model tracks 9 variables for a maximum of 4458 "cells", where one variable is the number of cells that the cell has divided into; in this way, the STORE.2 model can be thought of as modelling cell lineages.

6.5. Conclusion

Currently, c-MYC parameters are deterministic, with each daughter cell being complete clones of each other. c-MYC parameters should have corresponding probability distributions that determine, for example, the efficacy of amino acid influx. This will provide increased stochasticity to the STORE.2 model and reflect the fact that daughter cells are not perfect mathematical clones of one another.

Further work will need to introduce differentiation into the model, as T cells specialize to create different effector subtypes, and memory cells. Additionally, while the STORE.2 model can simulate division cessation, it cannot truly simulate the contraction phase. Measures of apoptosis will need to be introduced, chiefly Bcl-2, BIM, and Survivin.[10,11] CD8+ proliferation peaks around 7 days, whereupon T cells begin to die during the contraction phase.[12]

Despite this, the STORE.2 model is the first to simulate the master-cell cycle and metabolic regulator, c-MYC, for millions of individual cells, and the first to model the resulting impact on the

acidity of the extracellular microenvironment. It is also the first to model the positive and negative feedback loops that govern c-MYC. Finally, as in literature, division in the STORE.2 model is tempered by c-MYC depletion due to acidification and degradation mechanisms, as opposed to the STORE.1 model where cells would divide endlessly.

It does not sacrifice accuracy for explanatory power, having demonstrated an ability to accurately simulate in vivo WT and KO cell generation data up to 170 hours.

While the STORE.1 model simulated cell division via three different probability distributions. One for BP cells transitioning to C cells based on a 24-hour maturation time, one for C to I generation cells based around a 5-hour division time, and one for J generation cells based on a 24 hour division time. Division duration in the STORE.2 model

varies according to the evolution of cell and population dynamics, rather than being tied to three separate probabilities. Furthermore, in providing a mechanism for division cessation, the STORE.2 model predicts that the end of the proliferative phase occurs around 260-270 hours for WT-residing cells, and 280-290 hours for KO residing cells.

Perhaps most importantly, the STORE.2 model serves as a proof of concept. The logical structure is valuable in and of itself, that as the field of computational biology advances, models, including this one, can continue to integrate immunological mechanisms. Greater explanatory power is key to the ultimate goal of replicating the human immune response in a computer, a goal that promises to address the resource and time-limitations of vaccine development. I am proud that the STORE.2 model can serve as a small step towards it.

6.6. References

1) Zhan, Yifan, Emma M. Carrington, Yuxia Zhang, Susanne Heinzel, and Andrew M. Lew. “Life and Death of Activated T Cells: How Are They Different from Naïve T Cells?” *Frontiers in Immunology* 8 (December 13, 2017). https://doi.org/10.3389/fimmu.2017.01809.
2) Jorgensen, Trine N., Amy McKee, Michael Wang, Ella Kushnir, Janice White, Yosef Refaeli, John W. Kappler, and Philippa Marrack. “Bim and Bcl-2 Mutually Affect the Expression of the Other in T Cells.” *The Journal of Immunology* 179, no. 6 (September 4, 2007): 3417–24. https://doi.org/10.4049/jimmunol.179.6.3417.
3) Mitchell, Tom, John Kappler, and Philippa Marrack. “Bystander Virus Infection Prolongs Activated T Cell Survival.” *The Journal of Immunology* 162, no. 8 (April 15, 1999): 4527–35. https://doi.org/10.4049/jimmunol.162.8.4527.
4) Kurtulus, Sema, Pulak Tripathi, Maria E. Moreno-Fernandez, Allyson Sholl, Jonathan D. Katz, H. Leighton Grimes, and David A. Hildeman. “Bcl-2 Allows Effector and Memory CD8+ T Cells to Tolerate Higher Expression of Bim.” *Journal of Immunology (Baltimore, Md. : 1950)* 186, no. 10 (May 15, 2011): 5729–37. https://doi.org/10.4049/jimmunol.1100102.
5) Murphy, Daniel J., Melissa R. Junttila, Laurent Pouyet, Anthony Karnezis, Ksenya Shchors, Duyen A. Bui, Lamorna Brown-Swigart, Leisa Johnson, and Gerard I. Evan. “Distinct Thresholds Govern Myc’s Biological Output in Vivo.” *Cancer Cell* 14, no. 6 (December 2008): 447–57. https://doi.org/10.1016/j.ccr.2008.10.018.
6) Dang, Chi V. “C-Myc Target Genes Involved in Cell Growth, Apoptosis, and Metabolism.” *Molecular and Cellular Biology* 19, no. 1 (January 1, 1999): 1–11. https://www.ncbi.nlm.nih.gov/pmc/articles/PMC83860/.
7) Madden, Sarah K., Aline Dantas de Araujo, Mara Gerhardt, David P. Fairlie, and Jody M. Mason. “Taking the Myc out of Cancer: Toward Therapeutic Strategies to Directly Inhibit C-Myc.” *Molecular Cancer* 20, no. 1 (January 4, 2021). https://doi.org/10.1186/s12943-020-01291-6.
8) Zhou, Zi-Qiang, and Peter J Hurlin. “The Interplay between Mad and Myc in Proliferation and Differentiation.” *Trends in Cell Biology* 11, no. 11 (November 2001): S10–14. https://doi.org/10.1016/s0962-8924(01)02121-3.

9) Amati, Bruno, and Hartmut Land. “Myc—Max—Mad: A Transcription Factor Network Controlling Cell Cycle Progression, Differentiation and Death.” *Current Opinion in Genetics & Development* 4, no. 1 (February 1994): 102–8. https://doi.org/10.1016/0959-437x(94)90098-1.
10) Zhao, Baohua, Aihua Song, Rizwanul Haque, Fengyang Lei, Lauren Weiler, Xiaofang Xiong, Yuzhang Wu, Michael Croft, and Jianxun Song. “Co-Operation Between Molecular Targets Of Costimulation In Promoting T Cell Persistence And Tumor Regression.” *Journal of Immunology (Baltimore, Md. : 1950)* 182, no. 11 (June 1, 2009): 6744–52. https://doi.org/10.4049/jimmunol.0804387.
11) Heinzel, Susanne, Tran Binh Giang, Andrey Kan, Julia M. Marchingo, Bryan K. Lye, Lynn M. Corcoran, and Philip D. Hodgkin. “A Myc-Dependent Division Timer Complements a Cell-Death Timer to Regulate T Cell and B Cell Responses.” *Nature Immunology* 18, no. 1 (January 1, 2017): 96–103. https://doi.org/10.1038/ni.3598.
12) Prlic, M., and M. J. Bevan. “Exploring Regulatory Mechanisms of CD8+ T Cell Contraction.” *Proceedings of the National Academy of Sciences* 105, no. 43 (October 22, 2008): 16689–94. https://doi.org/10.1073/pnas.0808997105.